Chemical Engineering Journal Advances 7 (2021) 100125

Contents lists available at ScienceDirect

Chemical Engineering Journal Advances

journal homepage: www.elsevier.com/locate/ceja

Biohydrogen-producing from bottom to top? Quali-quantitative characterization of thermophilic fermentative consortia reveals microbial roles in an upflow fixed-film reactor

Lucas Tadeu Fuess [a,b,*], Laura Fuentes [c], Patricia Bovio-Winkler [c], Felipe Eng [b], Claudia Etchebehere [c], Marcelo Zaiat [b], Claudio Augusto Oller do Nascimento [a]

[a] Chemical Engineering Department, Polytechnic School, University of São Paulo. Av. Prof. Lineu Prestes, 580, Bloco 18 – Conjunto das Químicas, 05508-000, São Paulo, SP, Brasil

[b] Biological Processes Laboratory, São Carlos School of Engineering, University of São Paulo (EESC/USP), Av. João Dagnone 1100, São Carlos, SP 13563-120, Brazil

[c] Microbial Ecology Laboratory, Department of Biochemistry and Microbial Genomics, Biological Research Institute "Clemente Estable," 3318 Italia Avenue, Montevideo, Uruguay

ARTICLE INFO

Keywords:
16S rRNA gene sequencing
AnSTBR
Capnophilic lactic fermentation
Specific organic loading rate
Sugarcane biorefinery

ABSTRACT

Understanding specificities of biohydrogen ($bioH_2$)-producing systems is a key factor to enable efficient energetic exploitation of organic substrates in dark fermentation systems. The use of fixed-film reactors has been pointed as a determining approach to enhance $bioH_2$ evolution due to maintaining high cell densities within reactors. However, limiting substrate availability by excess cell accumulation has been associated with low hydrogenogenic activity levels due to stimulating $bioH_2$-consuming or non-producing pathways. A compartmentalized assessment was used to discover the dynamics of substrate conversion, cell retention patterns and the microbial characterization in different zones of a thermophilic (55 °C) molasses-fed fixed-film reactor under an organic loading rate of 20.0 kg-COD m^{-3} d^{-1}. Results indicated that microbial populations (e.g. *Thermoanaerobacterium* genus) in the basal portion of the reactor governed $bioH_2$ production by acetic- and butyric-type fermentation from sugars so that localized substrate availability (3.71 ± 1.13 g-COD g^{-1}VSS d^{-1}) reached favorable levels for $bioH_2$-producing populations. Lactate production by the *Janthinobacterium* genus occurred only as a secondary metabolic pathway in the bed-region, in which complementary $bioH_2$ production by the co-fermentation of acetate and lactate (also by *Thermoanaerobacterium* genus) was identified. The obtained results provide insights to manage the operation, as well as the design of acidogenic systems, indicating where and why $bioH_2$-producing populations prevail in fixed-film reactors.

1. Introduction

Biohydrogen ($bioH_2$) production in dark fermentation (DF) systems is dependent on a series of factors, such as the type of substrate, inoculum source and pretreatment, pH, temperature, carbon-to-nitrogen (C/N) ratio, provision of buffering conditions, nutrient supplementation, reactor configuration [1,2], among additional secondary aspects. In particular, reactor configurations are directly associated with the biomass retention capacity of fermentative systems, which usually define the success (or failure) of the process. Overall, higher cell retention capacities should lead to enhanced $bioH_2$ production levels [3], highlighting the advantage of fixed-film reactors over suspended cell growth-based

Abbreviations: AnSTBR, anaerobic structured-bed reactor; APBR, anaerobic packed-bed reactor; ASV, amplicon sequence variants; $BioH_2$, biohydrogen; BPP, biohydrogen production potential; C/N, carbon-to-nitrogen; CHt, total carbohydrates; CLF, capnophilic lactic fermentation; COD/Ca, COD-to-calcium; CODs, soluble chemical oxygen demand; CODt, total chemical oxygen demand; CRC, cell retention capacity; DF, dark fermentation; EC_{CHt}, CHt conversion efficiency; EtOH, ethanol; F/M, food-to-microorganism; FDC, feeding chamber; FHL, formate hydrogen lyase; FID, flame ionization detector; GC, gas chromatography; HAc, acetic acid; HBu, butyric acid; HLa, lactic acid; HPr, propionic acid; HRT, hydraulic retention time; HY, hydrogen yield; *hyd*, Fe-hydrogenase; LDPE, low-density polyethylene; NCBI, National Center for Biotechnology Information; OLR, organic loading rate; OTC, outlet chamber; PBS, phosphate buffered saline; RA, relative abundance; sOLR, specific organic loading rate; SPMB, soluble phase mass balance; SRT, solids retention time; STB_{LP}, structured-bed (lower portion); STB_{UP}, structured-bed (upper portion); TCD, thermal conductivity detector; UASB, upflow anaerobic sludge blanket (reactor); VFA, volatile fatty acids; VSS, volatile suspended solids; $Y_{X/S}$, biomass growth yield.

* Corresponding author.
E-mail addresses: ltfuess@alumni.usp.br (L.T. Fuess), felipe.eng@usp.br (F. Eng), cetchebehere@iibce.edu.uy (C. Etchebehere), zaiat@sc.usp.br (M. Zaiat), oller@usp.br (C.A. Oller do Nascimento).

https://doi.org/10.1016/j.ceja.2021.100125
Received 12 March 2021; Received in revised form 17 May 2021; Accepted 18 May 2021
2666-8211/© 2021 The Authors. Published by Elsevier B.V. This is an open access article under the CC BY license (http://creativecommons.org/licenses/by/4.0/)

systems by preventing an enhanced biomass washout [4]. This characteristic results from decoupling the solids retention time (SRT) from the hydraulic retention time (HRT) [3], which enables maintaining high cell densities within the systems.

However, practical results systematically show that excess biomass accumulation in DF systems negatively impacts long-term bioH_2 production [5-9] by unbalancing the food-to-microorganism (F/M) ratio in the reactor [4,5,10]. Substrate shortage conditions are observed under high biomass concentrations, which may shift the metabolic pathways from bioH_2-producing to non-bioH_2-producing or bioH_2-consuming conditions [8]. Studies frequently report on the establishment of homoacetogenic conditions (Wood-Ljungdahl pathway – Reaction 1 [11]) under low substrate availability in fermentative systems [6,12,13]. Increasing the applied organic loading rate (OLR) may comprise a strategy to overcome those metabolic shifts by properly maintaining adequate F/M values [14,15]; however, organic overloading conditions may trigger propionic- (Reaction 2) or lactic-type (Reaction 3) fermentation pathways [11], in which bioH_2 production is null.

$$4H_2 + 2CO_2 \rightarrow CH_3COOH + 2H_2O \quad \text{(Reaction 1)}$$

$$C_6H_{12}O_6 + H_2 \rightarrow 2CH_3CH_2COOH + 2H_2O \quad \text{(Reaction 2)}$$

$$C_6H_{12}O_6 \rightarrow 2CH_3CH(OH)COOH \quad \text{(Reaction 3)}$$

The specific organic loading rate (sOLR) has been reported as a parameter to calculate biomass retention levels in continuous DF systems [5], providing a relatively accurate estimate of the F/M ratio over time. Numerous applications of this methodological approach enabled correlating system performance with the evolution of biomass retention in both bioH_2-producing [4–6,8,16] and conventional methane-producing [17] reactors, in order to point out conditions of organic under- and overloads. However, this methodology assumes a homogeneous biomass concentration within the reactor, regardless of the flow pattern and system configuration. Compositional variations in the substrate inside the reactor are not considered either, as the term “food” in the F/M ratio corresponds to the influent organic source (e.g. carbohydrates). This particular aspect limits identifying bioH_2-producing zones in the systems.

This study investigates aspects of the distribution of the fermentative biomass in a continuous fixed-film DF reactor fed with sugarcane molasses under thermophilic (55 °C) conditions. Specifically, both the biomass distribution and the microbial characterization were performed by the end of the operating period. The sOLR at different zones of the reactor was innovatively obtained and compared with the conventional calculation approach, which assumes homogeneous biomass and substrate distributions. Finally, the bioH_2 production potential of the biomass collected from the different portions of the reactor was assessed. Overall, bioH_2-producing regions and the primary microbial groups were identified, providing a detailed understanding of the metabolic interactions in sugarcane molasses DF.

2. Material and methods

2.1. Fixed-film reactor: overall characteristics and sampling procedures

A bench-scale (1.9 L) anaerobic structured-bed reactor (AnSTBR) was continuously monitored for 320 d under thermophilic conditions (55 °C). The reactor was initially fed with sugarcane juice (days 1–179) and then with molasses (days 180–320) under diversified operating conditions, which aimed primarily to define optimal pH values for molasses fermentation at an OLR of approximately 20.0 kg-CODt m^{-3} d^{-1} (CODt = total chemical oxygen demand) and an HRT of 6 h. The impacts of the operating strategies applied in the AnSTBR over the long-term bioH_2 production are reported in detail elsewhere [18]. Following previous research [19], disassembling the reactor was based on draining the bulk liquid in four different regions, namely,

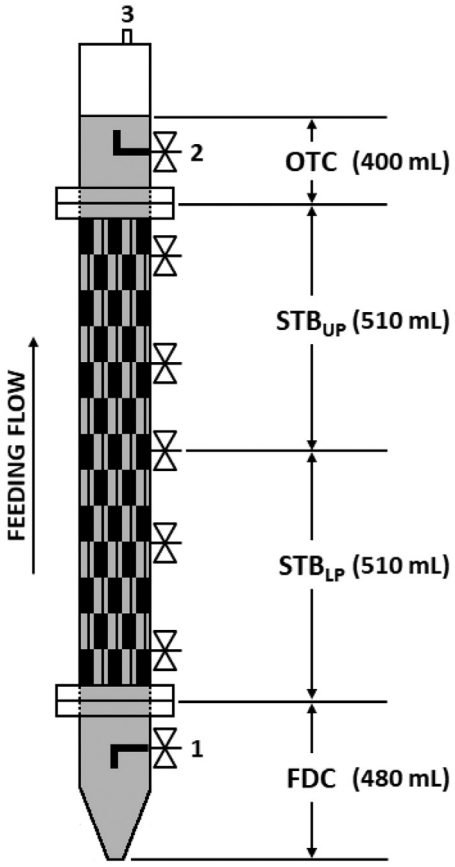

Fig. 1. Compartmentalization of the AnSTBR: FDC – feeding chamber, STB_{LP} – structured-bed (lower portion), STB_{UP} – structured-bed (upper portion) and OTC – outlet chamber. Legend: 1- influent port, 2- effluent port, 3- gas outlet.

feeding chamber (FDC), lower (STB_{LP}) and upper (STB_{UP}) portions of the structured-bed, and outlet chamber (OTC), from which biomass (as volatile suspended solids – VSS) and metabolite concentrations were determined (Section 2.3). Biomass attached to the structured-bed (low-density polyethylene – LDPE – rings), internal walls and screens (used to hold the support material) were also collected for VSS determination, following the previously defined STB_{LP} and STB_{UP} regions. Fig. 1 depicts an overview of the four different regions considered in the AnSTBR.

2.2. BioH$_2$ production potential (BPP) tests: assembly and monitoring

BPP tests were carried out in 500 mL Duran® flasks in batch mode. The flasks were filled with 300 mL of diluted molasses (CODt = 5 g L^{-1}) and inoculated with biomass collected from different regions of the AnSTBR: FDC, STB_{LP} and STB_{UP}. An F/M ratio of 3.70 g-CODt g^{-1}VSS was fixed in all conditions aiming to guarantee equivalent substrate availability per amount of inoculum. Controlling the buffer system of the reactors was achieved by dosing sodium bicarbonate (0.40 g-$NaHCO_3$ g^{-1}CODt) to maintain adequate pH values, as previously defined elsewhere [18]. The flasks were placed in a shaker (Model 430, Nova Ética, Vargem Grande Paulista, SP, Brazil) and maintained at controlled temperature (55 °C) and agitation (130–140 rpm) conditions. Prior to the incubation, the flasks were flushed with N_2 for 5 min to guarantee the establishment of an anaerobic environment, after which the reactors were sealed with bromobutyl rubber stoppers and plastic caps. Triplicates were monitored for each type of biomass, totalizing nine reactors.

Reactor monitoring was based on the periodic sampling of the gas phase for internal pressure and biogas composition measurements. The determination of the internal pressure was carried out with a pressure gauge (Model MDD50, T&S Equipamentos Eletrônicos, São Carlos, SP,

Brazil). Biogas sampling was carried out using 1000 μL insulin syringes equipped with Teflon body two-way valves (Supelco™ Analytical – Sigma-Aldrich, Bellefonte, PA, USA). In both procedures access to the headspace of the reactors was achieved using small gauge needles (24 G; 20 × 0.55 mm), i.e., the flasks were maintained sealed throughout the entire incubation period. The composition of the liquid phase was assessed only by the end of the incubation periods, based on the methodological procedures described in Section 2.3.

BioH_2 production was calculated following Eqs. (1)–(4), which describe the biogas production Eq. (1)), the bioH_2 production (Eq. (2)), the cumulative bioH_2 production and the molar bioH_2 production (Eq. (4)). In Eq. (1)–((4), the terms BGP_n, $P_{pre\text{-}injection,n}$, $P_{post\text{-}injection,n\text{-}1}$, BHP_n, $fH_{2,n}$, $BHP_{cum,n}$, $n_{H2,n}$, $V_{headspace}$, R and T are, respectively, the biogas production at time "n" (atm), the internal pressure measured prior to sampling at time "n" (atm), the internal pressure measured after the sampling at time "n – 1″ (atm), the bioH_2 production at time "n" (atm), the fraction of hydrogen in biogas at time "n" (dimensionless), the cumulative bioH_2 production up to time "n" (atm), the number of moles of hydrogen at time "n" (mol), the volume of the headspace (L), the universal gas constant (0.082 atm L mol^{-1} K^{-1}) and the incubation temperature (55 °C = 328.15 K).

$$BGP_n = P_{pre-injection,n} - P_{post-injection,n-1} \quad (1)$$

$$BHP_n = BGP_n \cdot fH_{2,n} \quad (2)$$

$$BHP_{cum,n} = \sum_{t=0}^{t=n} BHP_t \quad (3)$$

$$n_{H2,n} = \frac{BHP_{cum,n} \cdot V_{headspace}}{R \cdot T} \quad (4)$$

The modified Gompertz model [20] was fitted to the molar bioH_2 production profiles to obtain the potential bioH_2 production (P_{H2}; mol or mmol), the maximum bioH_2 production rate (R_{H2}; mol h^{-1} or mmol h^{-1}) and the lag phase period (λ; h) according to Eq. (5). In Eq. (5), the terms $n_{H2}(t)$ and e are respectively the molar bioH_2 production as a function of the incubation time (t) and the Euler's number (2.71828). The kinetic parameters were obtained using the software OriginPro 8 (OriginLab Corporation, Northampton, MA, USA) by using the Levenberg-Marquardt algorithm.

$$n_{H2}(t) = P_{H2} \cdot \exp\left\{-\exp\left[\frac{R_{H2} \cdot e}{P_{H2}}(\lambda - t) + 1\right]\right\} \quad (5)$$

2.3. Analytical methods: biogas and liquid phase determinations

Biogas composition (H_2, N_2, CH_4 and CO_2) in BPP tests was carried out by gas chromatography (model GC-2010, Shimadzu Scientific Instruments, Japan) using a thermal conductivity detector (TCD) and argon as the carrier gas [15]. The bulk liquid drained from the AnSTBR at different portions and the fermented molasses remaining after the BPP tests were characterized in terms of the pH, soluble COD (CODs), total carbohydrates (CHt), lactic acid (HLa), volatile fatty acids (VFA; C2–C6) and solvents. VSS measurements were carried out to specifically quantify biomass concentrations in the bulk liquid and support media (AnSTBR), as indicated in Section 2.1. pH, CODs and VSS measurements were carried out according to the Standard Methods for the Examination of Water and Wastewater [21]. CHt, HLa and VFA/solvent concentrations followed protocols described by Dubois et al. [22], Taylor [23] and Adorno et al. [24], respectively. VFA/solvent determinations were carried out using a GC set (model GC-2010, Shimadzu Scientific Instruments, Japan) equipped with a flame ionization detector (FID) and a COMBI-PAL auto sampler. Hydrogen, synthetic air and nitrogen were used as the carrier, flame and make-up gases, respectively. The samples were filtered in 0.45 μm filters (Chromafil GF/PET, Macherey-Nagel GmbH & Co. KG, Düren, Germany) prior to CODs, CHt, HLa and VFA/solvent analyses.

Primary calculations used to assess systems' performance (specifically for BPP tests) included determining the hydrogen yield (HY; mmol g^{-1}CHt) and the CHt conversion efficiency (EC_{CHt}; %). The reliability of the soluble phase measurements (bulk liquid of the AnSTBR and fermented substrates in BPP tests) was also assessed by calculating a soluble phase mass balance (SPMB) considering the following compounds and their respective factors of COD equivalence: CHt (as glucose; 1.06 g-COD g^{-1}CHt), HLa (1.07 g-COD g^{-1}HLa), ethanol (EtOH; 2.09 g-COD g^{-1}EtOH), acetic acid (HAc; 1.07 g-COD g^{-1}HAc), propionic acid (HPr; 1.51 g-COD g^{-1}HPr) and butyric acid (HBu; 1.82 g-COD g^{-1}HBu).

2.4. sOLR: conventional and segmented approaches

VSS measurements were further used to calculate the sOLR (conventional approach) as proposed elsewhere [5]. Eqs. (6)–(8) were initially used to obtain the overall biomass growth yield ($Y_{X/S}$; g-VSS g^{-1}CHt), in which the terms X_S, X_A, X_E, S_{CHt}, Q, VSS_E, CHt_I and CHt_E, are, respectively, the amount of suspended biomass in the bulk liquid of the reactor (g-VSS), the amount of biomass attached to the support media and other internal surface areas of the reactor (g-VSS), the total amount of biomass washed out in the effluent stream (g-VSS), the total amount of converted substrate (as CHt) during the entire operating period (g-CHt), the flow rate applied in the AnSTBR (L d^{-1}), the concentration of VSS in the effluent stream (g L^{-1}) and the concentrations of CHt in the influent and effluent streams (g L^{-1}). The term X_S represents the total amount of biomass measured in the bulk liquid of the reactor by the end of the operation considering all four specific regions, i.e., FDC, STB_{LP}, STB_{UP} and OTC (Fig. 1). The term X_A includes the biomass attached to the support media, internal walls and screens used to hold the structured-bed, also measured by the end of the operation.

$$Y_{X/S} = \frac{X_S + X_A + X_E}{S_{CHt}} \quad (6)$$

$$X_E = \int_0^t \left(Q \cdot VSS_E\right)dt \quad (7)$$

$$S_{CHt} = \int_0^t \left[Q \cdot \left(CHt_I - CHt_E\right)\right]dt \quad (8)$$

The calculation of the biomass concentration inside the reactor at a given time "n" (X_n as g-VSS L^{-1}; Eq. (9)) preceded the determination of the sOLR (g-CHt g^{-1}VSS d^{-1} or g-COD g^{-1}VSS d^{-1}; Eq. (10)) so that the terms Δt, V_u, X_{n-1} and OLR are, respectively, the time interval for which the biomass growth was considered (d), the working volume of the reactor (L), the concentration of biomass inside the reactor at the time "n – 1″ (g-VSS L^{-1}), and the applied organic loading rate (g-CHt L^{-1} d^{-1} or g-COD L^{-1} d^{-1}; following the COD-equivalent factor of 1.06 g-COD g^{-1}CHt).

$$X_n = \left[\frac{S_{CH} \cdot Y_{X/S} \cdot \Delta_t}{V_u} \cdot \left(\frac{X_S + X_A}{X_S + X_A + X_E}\right)\right] + X_{n-1} \quad (9)$$

$$sOLR = \frac{OLR}{X_n} \quad (10)$$

A complementary methodology was applied in the calculation of the sOLR following the segmentation of the reactor in different compartments (FDC, STB_{LP}, STB_{UP} and OTC). In this case, the biomass concentration within a given compartment ($X_n^{compartment}$; g-VSS L^{-1}) was calculated through Eq. (11), from which the sOLR in the respective compartment ($sOLR_{compartment}$; g-CHt g^{-1}VSS d^{-1} or g-COD g^{-1}VSS d^{-1}) was obtained Eq. (12)). In Eq. (11)–((12) the terms EC_{CHt}, $V_{compartment}$, $X_{compartment}$ and $X_{n\text{-}1}^{compartment}$ are, respectively, the CHt conversion efficiency in the portion immediately below the assessed compartment (dimensionless), the volume of the compartment (L; Fig. 1), the amount of biomass directly measured in the compartment by the end of the operation (g-VSS) and the concentration of biomass in the compartment at time "n – 1" (g-VSS L^{-1}). EC_{CHt} values were obtained from

the metabolite concentration profile by comparing sequential compartments (Section 2.1). Calculations for the FDC considered the CHt concentration measured in the raw substrate, i.e., $EC_{CHt} = 0$ (zero), whilst the effluent CHt concentration in the FDC was equivalent to the influent level in STB_{LP}, and so on.

$$X_n^{compartment} = \left[\frac{(1 - EC_{CHt}) \cdot S_{CHt} \cdot Y_{X/S} \cdot \Delta_t}{V_{compartment}} \cdot \left(\frac{X_{compartment}}{X_S + X_A + X_E}\right)\right] + X_{n-1}^{compartment} \quad (11)$$

$$sOLR_{compartment} = \frac{\frac{(1-EC_{CHt}) \cdot CHt \cdot Q}{V_{compartment}}}{X_n^{compartment}} \quad (12)$$

2.5. Molecular analyses

The characterization of the microbial communities was carried out in four samples (S1–S4), which corresponded to the sugarcane vinasse-derived inoculum (S1), the suspended biomass in the FDC (S2) and the attached biomass in the STB_{LP} (S3) and STB_{UP} (S4). S1 was collected after the natural fermentation procedure, specifically after the 5-day long recirculation of fermented vinasse into the AnSTBR. S2–S4 were collected by the end of the operation of the AnSTBR, following the compartmentalized disassembling of the reactor (Section 2.1). Procedures used in sample preparation (removal of impurities using a phosphate buffered saline, PBS), DNA extraction, 16S rRNA gene sequencing, data analysis (bioinformatics), and quantification of Fe-Fe hydrogenase by real time quantitative PCR (q-PCR) were equal to those described elsewhere [19]. A total number of 122,277 sequences were obtained, with individual values ranging between 19,633 and 45,780 sequences per sample ($nn = 4$), representing 283 amplicon sequence variants (ASV). Further downstream diversity and composition analyses were carried out using sequences rarified to the lowest amount per sample, i.e., 19,633 sequences. The sequences were submitted to the National Center for Biotechnology Information (NCBI; http://ncbi.nlm.nih.gov) under accession BioProject ID PRJNA663617 (SAMN16170514).

3. Results and discussion

3.1. AnSTBR: spatial metabolite distribution

Understanding the impacts of reactor's height on substrate (CHt) consumption and metabolite production was based on the characterization of samples collected from different compartments. The spatial metabolite distribution in the AnSTBR is depicted in Fig. 2a, b, indicating a sharp CHt consumption in the FDC (89.5%). This pattern most likely resulted from the biomass accumulation within the basal portion of the reactor (Section 3.2), which favored the establishment of $bioH_2$-producing populations (Section 3.3), providing minimal levels of fresh substrate to the attached biomass in the upper portions (STB_{LP} and STB_{UP}). Metabolite distribution showed a clear stratification, in which two distinct patterns were identified along the height of the AnSTBR: initial enhanced acetic- and butyric-type fermentation pathways (FDC) and a subsequent increase in the lactic activity in the structured-bed region (Fig. 2a, b). Major variations in the metabolite spatial profile were observed up to the STB_{LP}, from which the same distribution pattern was observed up to the effluent stream (Fig. 2a, b). HBu levels slightly varied toward the effluent port (910 ± 107 mg-COD), whilst HAc and HPr levels presented decreasing patterns, i.e., 594–115 mg-COD and 35–12 mg-COD, respectively (Fig. 2a). Variations in EtOH levels were relatively minimal along the entire height of the reactor (78 ± 13 mg-COD), indicating that some ethanolic activity was observed only in the lower portions of the reactor. pH measurements also indicated minimal variations along the different compartments (5.51–5.38), suggesting the establishment of well-balanced conditions for the production of $bioH_2$ from molasses based

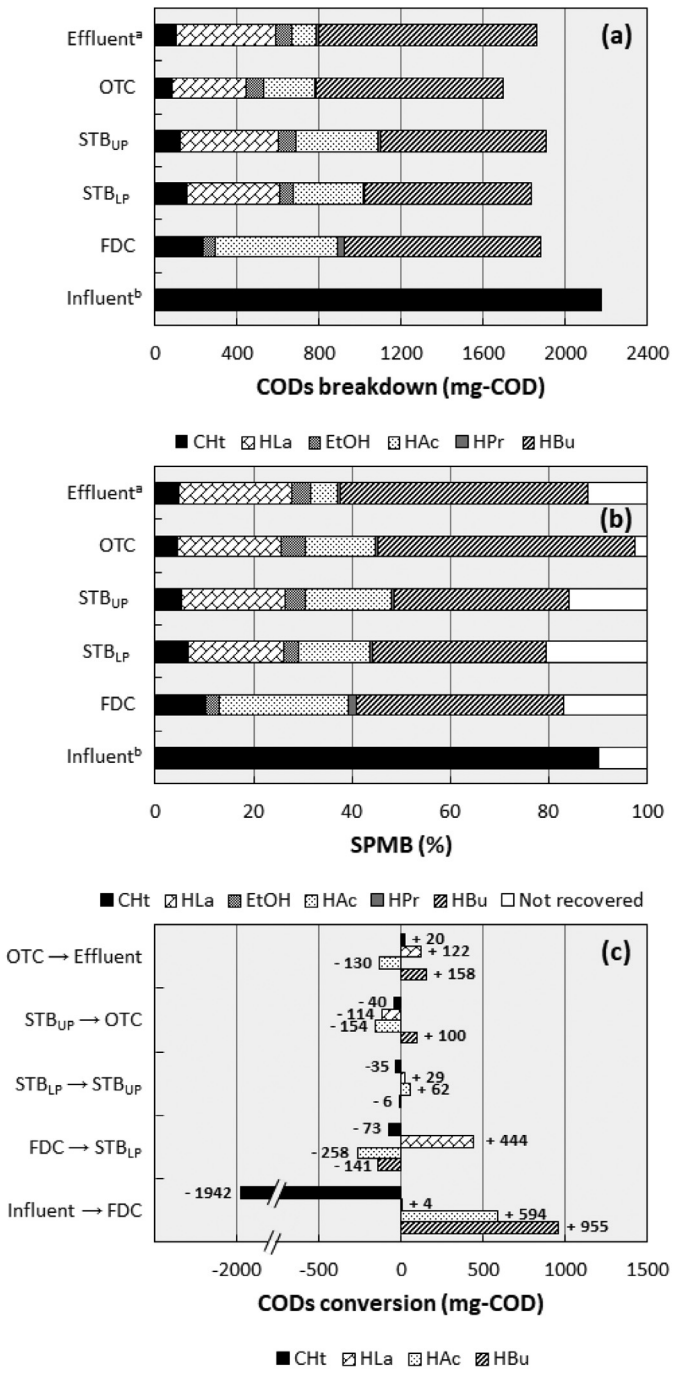

Fig. 2. Spatial distribution of metabolites along the AnSTBR: (a) metabolite concentration profile, (b) CODs-based SPMB and (c) CODs conversion patterns for selected metabolites between consecutive compartments. Notes: [a]Fermented molasses, [b]Raw (fresh) molasses. Nomenclature: FDC – feeding chamber, STB_{LP} – structured-bed (lower portion), STB_{UP} – structured-bed (upper portion), OTC – outlet chamber, CHt – total carbohydrates, HLa – lactic acid, EtOH – ethanol, HAc – acetic acid, HPr – propionic acid, HBu – butyric acid.

on the system optimization through $NaHCO_3$ dosing (0.40 g-$NaHCO_3$ g^{-1}CODt), as reported elsewhere [18].

The metabolite profile indicated both the acetic (Reaction 4 [11]) and butyric (Reaction 5 [11]) fermentation pathways as major $bioH_2$ production sources within the AnSTBR. Using the measured metabolite levels (Fig. 2a) and the stoichiometric (molar) relationships between $bioH_2$ and both HAc and HBu in Reactions (4) and (5) indicates a 3-fold higher $bioH_2$-producing potential (18.5 *vs.* 6.0 mmol) for the acetic-

type fermentation, which highlights the determining contribution of this particular pathway for the hydrogenogenic activity. This finding contradicts previous studies assessing acidogenic systems inoculated with naturally fermented sugarcane vinasse [16,25,26], which pointed out the co-fermentation of HLa and HAc as the major pathway to produce both $bioH_2$ and HBu (Reaction 6 [27]), irrespective of the substrate type (i.e., vinasse or molasses). Despite the consistency of such comparative results, which were primarily based on metabolic correlations [16,25], using only the metabolite profile for the effluent stream (temporal characterization) may not be representative for the overall conversion process.

$$C_6H_{12}O_6 + 2H_2O \rightarrow 2CH_3COOH + 4H_2 + 2CO_2 \quad \text{(Reaction 4)}$$

$$C_6H_{12}O_6 \rightarrow CH_3(CH_2)_2COOH + 2H_2 + 2CO_2 \quad \text{(Reaction 5)}$$

$$CH_3COOH + 2CH_3CH(OH)COOH \rightarrow H_2 + 3/2CH_3(CH_2)_2COOH + 2CO_2 + H_2O \quad \text{(Reaction 6)}$$

Comparing metabolite distribution patterns for both the FDC and the effluent stream (Fig. 2a, b) suggests two different $bioH_2$-producing fermentation dynamics within the AnSTBR, indicating a relatively low contribution of the acetic-type fermentation in the latter case. However, the marked CHt conversion observed in the FDC strongly highlights the production of HAc as a primary substrate during $bioH_2$ evolution from fresh substrate uptake. $BioH_2$ production through the co-fermentation of HLa and HAc (Reaction 6) may have occurred as a "residual" pathway only in the upper portions of the structured-bed region, as variations in the CODs conversion (Fig. 2c) showed increasing HBu levels coupled to the consumption of HLa and primarily HAc between the STB_{UP} and the OTC/effluent stream. A similar pattern was reported elsewhere [19], in which $bioH_2$ production from HLa and HAc was identified as a complementary pathway to direct sugar fermentation via acetic- (Reaction 4) and butyric-type (Reaction 5) fermentation.

HLa production in the structured-bed region (Fig. 2a, b) was not primarily associated with sugar fermentation (Reaction 3), given the low availability of CHt compared to the levels provided in the influent stream. The increase observed in HLa production (448 mg-COD) was over 6-fold higher than the decrease in CHt availability (73 mg-COD) when comparing metabolite distribution in the FDC and STB_{LP} (Fig. 2c), suggesting the establishment of alternative lactic activity sources. Capnophilic lactic fermentation (CLF) has been pointed out as a potential HLa-producing pathway in $NaHCO_3$-supplied molasses DF, as previously speculated in the long-term analysis of the temporal metabolite profiles of the AnSTBR [18]. CLF is triggered when proper concentrations of dissolved CO_2 are observed in the bulk liquid [28,29], in which pyruvate reduction is favored to the detriment of the oxidative decarboxylation. Along with CO_2, CLF recycles a fraction of the HAc available in the bulk liquid (Reaction 7 [29]) via acetyl-CoA through pyruvate:ferredoxin oxidoreductase enzyme [29], in which bacteria belonging to the genus *Thermotoga* usually play a key metabolic role [28,30]. In addition to the release of CO_2 from sugar fermentation (e.g. Reactions 4–6), the enhanced release of H^+ ions (production of HAc and HBu) in the FDC triggered the dissociation of $NaHCO_3$ in the buffering mechanism, increasing the availability of CO_2 in the upper portions of the AnSTBR, specifically in the immediately above portion of the bed region (STB_{LP}). Consequently, the high availability of both HAc and CO_2 stimulated the capnophilic behavior in a given microbial group, as detailed in Section 3.4.

$$CH_3COOH + CO_2 + 4H^+ + 4e^- \rightarrow CH_3CH(OH)COOH + H_2O \quad \text{(Reaction 7)}$$

CODs conversion patterns between the FDC and the STB_{LP} (Fig. 2c) indicated that approximately 60.0% of the produced HLa (444 mg-COD) resulted from HAc conversion (258 mg-COD), which may indicate a determining contribution of CLF. Complementarily, previous studies reported on increasing lactic activity in some *Lactobacillus* strains by adding acetate in glucose-fed fermentative systems [31-33]. Similarly, Khor et al. [34] also reported increasing patterns for HLa production from different organic substrates, i.e., cornstarch and extruded grass, by adding acetate to the fermentation broths. These previous findings indicate another potential source for the correlation between HAc consumption and HLa production observed in this study, although the *Lactobacillus* genus participated minimally in the composition of microbial samples (Section 3.4). The remaining fraction of HLa may have resulted from the catabolism of HBu (141 mg-COD in the transition between the FDC and the STB_{LP}; Fig. 2c), following a few previous findings. Enhanced conversion of HBu into HLa (~50%) has been reported to occur in the epithelium of the stomach (omasum) in ruminants [35]. HBu has been reported as a precursor of carbohydrates in dairy cow, acting as a substrate for lactose production [36], which may be hydrolyzed into glucose and galactose and further converted into HLa (Reaction 8 [37]).

$$C_{12}H_{22}O_{11} + H_2O \rightarrow C_6H_{12}O_6 + C_6H_{12}O_6 \rightarrow 4CH_3CH(OH)COOH \quad \text{(Reaction 8)}$$

Additional metabolic pathways potentially established within the AnSTBR could include the heterolactic fermentation, which also generates EtOH (Reaction 9 [38]). However, EtOH concentrations varied negligibly compared with HBu, HLa and HAc along the reactor (Fig. 2a, b), suggesting the occurrence of other pathways, such as the direct EtOH production (Reaction 10 [11]) or the co-production of EtOH, HAc and $bioH_2$ (Reaction 11 [39]) from sugar fermentation in the FDC. Finally, the minimum HPr concentrations identified in the STB_{UP} may have resulted from HLa (Reaction 12 [38]) or EtOH (Reaction 13 [40]) uptake, as the operation of the continuous reactor (OLR = 20 kg-CODt m^{-3} d^{-1}) was far from organic overloading conditions (OLR > 86 kg-CODt m^{-3} d^{-1}, as suggested by results reported elsewhere [18]), in which HPr production coupled to $bioH_2$ consumption (Reaction 2) is usually observed. Finally, the SPMB reached an average value of 87.0 ± 6.4% (79.3–97.4%; Fig. 2b), ensuring the reliability of the methodological protocols used. The undetected fractions (usually < 15.0%) were most likely composed by negligible levels of other organic acids and phenolic compounds.

$$C_6H_{12}O_6 \rightarrow CH_3CH(OH)COOH + CH_3CH_2OH + CO_2 \quad \text{(Reaction 9)}$$

$$C_6H_{12}O_6 \rightarrow 2CH_3CH_2OH + 2CO_2 \quad \text{(Reaction 10)}$$

$$C_6H_{12}O_6 + H_2O \rightarrow 2H_2 + 2CO_2 + CH_3CH_2OH + CH_3COOH \quad \text{(Reaction 11)}$$

$$3CH_3CH(OH)COOH \rightarrow 2CH_3CH_2COOH + CH_3COOH + CO_2 + H_2O \quad \text{(Reaction 12)}$$

$$3CH_3CH_2OH + CO_2 \rightarrow 2CH_3CH_2COOH + CH_3COOH + H_2O \quad \text{(Reaction 13)}$$

Finally, results from a similar compartmentalized assessment approach applied in another thermophilic molasses-fed AnSTBR [19] indicated a different pattern regarding metabolite distribution, most likely as a result of applying a 4-fold higher OLR (86.0 kg-CODt m^{-3} d^{-1}). In that case, HLa production occurred primarily in the FDC via direct sugar fermentation (Reaction 3), whilst decreasing HLa levels were observed along the bed region coupled to HBu and $bioH_2$ production by Reaction (6). Although acetic- (Reaction 4) and butyric-type (Reaction 5) fermentation from sugars largely contributed to the hydrogenogenic activity in the FDC, as observed herein, the co-fermentation of HLa and HAc (Reaction 6) played a more relevant role within the total hydrogenogenic activity at higher OLR levels [19]. These discrepant patterns indicate that the "protagonism" of active lactate-producing populations within acidogenic systems depends on the applied OLR. On the one hand, conditions

Table 1
Biomass distribution levels and biomass growth yield in different fixed-bed acidogenic reactors.

Biomass distribution (**mg-VSS**; *relative percentage*[a,b])				$Y_{X/S}$		
Attached	Suspended	Washed out[c]	Total	(g-VSS g^{-1}CHt)	Reactor	Reference
12,286 *(4.8%[a], 53.3%[b])*	**10,752** *(4.1%[a], 46,7%[b])*	**236,596** *(91.1%[a])*	**259,634** *(100.0%[a])*	0.056	AnSTBR	This study
23,700 *(22.2%[a], 84.3%[b])*	**4400** *(4.1%[a], 15.6%[b])*	**78,500** *(73.6%[a])*	**106,700** *(100.0%[a])*	0.040	APBR	[5][d] C/*N* = 40
12,900 *(20.3%[a], 66.8%[b])*	**6400** *(10.1%[a], 33.2%[b])*	**44,300** *(69.6%[a])*	**63,600** *(100.0%[a])*	0.030	APBR	[5][d] C/*N* = 140
8625 *(3.7%[a], 20.2%[b])*	**34,074** *(14.8%[a], 79.8%[b])*	**187,463** *(81.4%[a])*	**230,162** *(100.0%[a])*	0.051	AnSTBR	[41][e]

Abbreviations: AnSTBR- anaerobic structured-bed reactor, APBR- anaerobic packed-bed reactor, HRT- hydraulic retention time, OLR- organic loading rate, LDPE- low-density polyethylene. Values in **bold** correspond to the amount of biomass experimentally measured (mg-VSS).
Notes:
[a] Relative to the total produced biomass;.
[b] Relative to the retained biomass (attached + suspended);.
[c] Calculated from effluent VSS concentrations;.
[d] Operating conditions: HRT = 2 h, OLR = 24.0 kg-CODt m^{-3} d^{-1}, temperature = 25 °C, LDPE as the support material, operating period = 60 d;.
[e] Operating conditions: HRT = 2 h, OLR = 24.0 kg-CODt m^{-3} d^{-1}, temperature = 25 °C, LDPE as the support material, operating period = 90 d

of high OLR (or even organic overloading) stimulate enhanced HLa production from sugars as a primary pathway in high CHt availability, as described elsewhere [19]. Consequently, HLa-consuming pathways (e.g. Reaction 6) will be proportionally stimulated. On the other hand, HLa production will be a secondary pathway in the application of lower OLR levels (this study), and its further consumption will be limited due to the lower available levels.

3.2. Biomass distribution and sOLR calculation

Determining/quantifying biomass distribution inside continuous fixed-film reactors and the associated sOLR is a challenge, because direct measurements approaches are still poor to effectively differentiate the fractions of attached and suspended cells. Details of the biomass distribution within the AnSTBR by the end of the operation are presented in Fig. 3a and Table 1, based on the segmentation of the reactor previously defined, namely the feeding chamber (FDC), lower (STB_{LP}) and upper (STB_{UP}) portions of the structured-bed and outlet chamber (OTC) (Section 2.1). Equivalent amounts of solids were identified in the FDC (10,283 mg-VSS or 44.6%) and structured-bed (lower and upper portions, 10,370 mg-VSS or 45.0%), whilst minimal values were measured in the OTC (133 mg-VSS or 0.6%) (Fig. 3a). A slightly higher biomass amount was measured in the STB_{LP} (5793 mg-VSS) compared with the STB_{UP} (4577 mg-VSS), most likely as a result of the input of higher residual levels of fresh substrate (CHt). Considering the application of equivalent operating conditions (substrate type and concentration, OLR and HRT [18]) for 140 days, it is plausible to indicate that the obtained biomass distribution is representative for the considered operating period. The relatively stable effluent VSS concentrations measured within the period, i.e., 122–140 mg L^{-1} [18], corroborate this hypothesis, indicating no clear disturbance in biomass washout.

The total amount of biomass retained in the system and measured by the end of the operating period (23,038 mg-VSS; experimental value) was equivalent to the value estimated through the sOLR calculation methodology (25,479 mg-VSS) (Fig. 3b). In particular, the temporal profile showing the evolution of biomass retention indicated two distinct patterns (days 1–179 and 180–320; Fig. 2b), directly reflecting the behavior of the acidogenic system (in terms of biomass production) in response to using distinct substrates, namely, sugarcane juice (days 1–179) and molasses (days 180–320) [18]. Nitrogen deficiency was identified as a critical aspect impairing both the $bioH_2$ production and CHt conversion from juice, most likely by limiting the cell growth within the AnSTBR [18]. The obtained biomass retention profile (Fig. 2b) supports the hypothesis previously highlighted so that the increase in biomass retention (day 180 onwards; Fig. 2b) may be explained by the sharp increase in the CHt conversion observed, i.e., 17.0–49.4% (days 1–179) *vs.* 86.2–94.3% (days 180–320) [18]. The biomass retention rate, which was obtained through fitting (and further deriving) linear equations (data not shown) to the experimental values at each specific period, was almost 2.5-fold higher for molasses compared with juice (54.1 *vs.* 22.0 mg-VSS d^{-1}).

The literature lacks data on the cell distribution in $bioH_2$-producing acidogenic systems, although some studies reported on the amount of biomass by the end of operating runs (Table 1). The cell retention capacity (CRC) within the fixed-film region, i.e., 45.0% (considering both attached and suspended fractions; Fig. 3a) of the total retained biomass, was higher than the previously reported one by Anzola-Rojas and Zaiat [41], i.e., 20.2% (Table 1), also considering the operation of structured-bed systems. The observed discrepancy may have resulted from differences in the overall operating period (320 days *vs.* 90 days), applied HRT (24–6 h *vs.* 2 h) and feeding strategy (upflow *vs.* downflow), which makes it difficult to make a direct comparison. Nevertheless, CRC values observed for the AnSTBR are lower than in packed-bed systems, in which values ranged between 66.8–84.3% according to the availability of nitrogen [5] (Table 1). Aquino et al. [17] reported a similar trend when comparing the application of packed- and structured-bed reactors in the methanogenesis of vinasse, calculating a 3-fold higher CRC in the first system (36.4 *vs.* 13.2%). Considering differences in biomass washout levels corroborates the observed patterns, as over 80.0% of the total production of solids was naturally eliminated in AnSTBR systems, with lower values (69.6–73.6%) associated with packed-bed ones (Table 1).

Analyzing the $Y_{X/S}$ values for anaerobic populations also provides a good understanding of the CRC within the fixed-film systems. Overall, the more favorable the conditions provided for biomass attachment, the lower the $Y_{X/S}$, as less energy is directed to biomass growth [17]. Favoring biomass attachment, i.e., higher CRC values, enables maintaining a high cell activity within the reactors, whilst enhanced biomass washout conditions (lower CRC) require higher cell growth rates to offset the losses in cell activity. Physiological modifications in biofilm-forming cells, which may result from increasing local nutrient concentrations [42], explain these different growth levels. Comparing $Y_{X/S}$ values for packed- and structured-bed reactors clearly corroborates this pattern, as the values calculated for the latter (0.051–0.056 g-VSS g^{-1}CHt; Table 1) are 1.3–1.9-fold higher than in the first (0.030–0.040 g-VSS g^{-1}CHt;

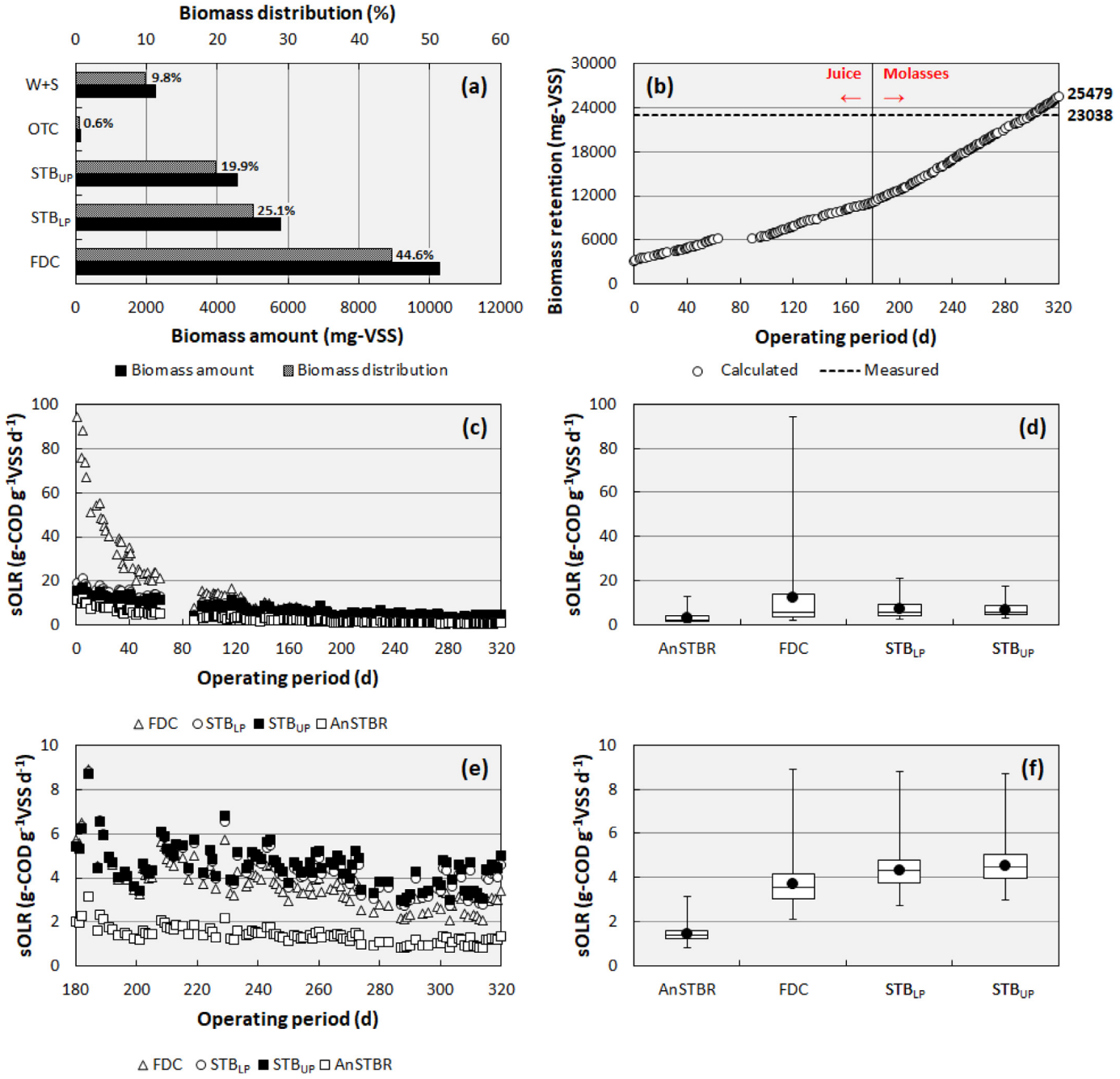

Fig. 3. Biomass balance within the different compartments of the AnSTBR: (a) spatial biomass distribution, (b) evolution of biomass retention, (c) temporal profile (days 1–320) of the sOLR, (d) overall variation of the sOLR (days 1–320), (e) temporal profile of the sOLR when using molasses as the substrate (days 180–320) and (f) variation of the sOLR when using molasses as the substrate (days 180–320). Nomenclature: FDC – feeding chamber, STB_{LP} – structured-bed (lower portion), STB_{UP} – structured-bed (upper portion), OTC – outlet chamber, W + S – walls + screens.

Table 1), irrespective of the operating conditions. Blanco et al. [6] also reported a similar pattern when comparing bioH_2-producing AnSTBR systems subjected to different COD-to-calcium (COD/Ca) ratios, indicating that the higher the calcium concentration (lower COD/Ca ratio), the lower the $Y_{X/S}$, because calcium favors biomass retention. In the same context, Gomes et al. [4] reported $Y_{X/S}$ values as high as 0.06–0.08 g-VSS g^{-1}sucrose in the operation of a continuous multiple tube reactor, characterized by an enhanced cell washout due to the absence of support materials for biomass attachment.

Considering the assessment of the sOLR, applying a different calculation approach through reactor compartmentalization allowed understanding how substrate availability varies within the acidogenic system (Fig. 3c,f). In this case, special focus was given to the period in which molasses was used as the organic substrate, as highlighted in Fig. 3e,f. The sOLR calculated using the conventional approach [5] narrowly varied within the last 140 operating days (1.41 ± 0.38 g-COD g^{-1}VSS d^{-1}), characterizing a value at least 3-fold lower than the optimal sOLR range associated with favorable bioH_2 production levels, i.e., 4.40–7.18 g-COD g^{-1}VSS d^{-1} [5,8,10]. This fact characterizes a conflicting pattern, as a sharp improvement was observed in bioH_2 production in the AnSTBR during the considered operating period (days 180–320 [18]). However, the analysis of the sOLR in each compartment of the reactor (FDC = 3.71 ± 1.13 g-COD g^{-1}VSS d^{-1}, STB_{LP} = 4.33 ± 0.97 g-COD g^{-1}VSS d^{-1} and STB_{UP} = 4.53 ± 0.92 g-COD g^{-1}VSS d^{-1}) suggests the

Table 2
Kinetic parameters and performance summary of the fermentation in BPP tests.

Compartment		FDC	STB_{LP}	STB_{UP}	
Kinetic parameters	P_{H2} (mmol)	6.14 ± 0.10	2.87 ± 0.05	2.80 ± 0.15[a]	4.13 ± 0.10[b]
	R_{H2} (mmol h^{-1})	0.78 ± 0.07	0.12 ± 0.01	0.17 ± 0.02[a]	0.09 ± 0.00[b]
	λ (h)	14.11 ± 0.41	5.58 ± 0.65	4.86 ± 1.31[a]	0[b]
	R^2	0.978	0.988	0.942[a]	0.941[b]
EC_{CHt} (%)		94.7 ± 0.3	94.8 ± 0.5	95.4 ± 0.2	
HY (mmol g^{-1}CHt)		5.23 ± 0.26	2.48 ± 0.05	3.21 ± 0.04	
pH (-)		5.58 ± 0.49	4.61 ± 0.18	4.66 ± 0.11	

Abbreviations/symbols: P_{H2} - potential bioH2 production, R_{H2} - maximum $bioH_2$ production rate, λ - lag phase, EC_{CHt} - total carbohydrates conversion efficiency, HY - hydrogen yield.
Notes:
[a] Period: 0–36 h.
[b] Period: 36–59 h.

local establishment of suitable conditions for $bioH_2$ production (Fig. 3f). In particular, maintaining adequate sOLR values in the FDC most likely favored the establishment of populations with high $bioH_2$ production capabilities, explaining the patterns further discussed in Section 3.3.

Therefore, calculating the sOLR using the proposed approach herein was imperative to understand the dynamics of $bioH_2$ production in fixed-film acidogenic reactors, as considering a homogeneous biomass and substrate distribution masks the interpretation of the metabolic role of the different acidogenic populations. The sOLR in the OTC reached extremely high values (305 ± 98 g-COD g^{-1}VSS d^{-1}) as a direct result of the low biomass concentration (Fig. 2a). The proposed methodology also enabled to calculate the sOLR in terms of both HBu (19.20 ± 4.31 g-COD g^{-1}VSS d^{-1}; days 180–320) and HAc (11.95 ± 2.68 g-COD g^{-1}VSS d^{-1}; days 180–320) in the STB_{LP}, reaching values at least 2.7-fold higher than CHt availability. This fact corroborates the relevance of both substrates to provide metabolic energy to guarantee the growth of approximately 25% (Fig. 3a) of the biomass retained within the AnSTBR.

3.3. BPP tests: where does $bioH_2$ production occur?

The impacts of metabolite/biomass stratification along the height of the AnSTBR on the hydrogenogenic activity were assessed in BPP tests by incubating biomass samples collected from different compartments. Details of the BPP tests regarding both the molar $bioH_2$ production (experimental and fitted models) and metabolite concentration profiles are depicted in Fig. 4a,c, whilst the kinetic parameters and overall performance data are summarized in Table 2. Overall, $bioH_2$ production presented a single kinetic pattern, except for the STB_{UP}, in which two behaviors were identified, namely, between 0 and 36 h and 36–59 h (Fig. 4a and Table 2). Nevertheless, the potential $bioH_2$ production of the biomass collected from the FDC was at least 1.5-fold higher (6.14 *vs.* 2.80–4.13 mmol) than those of biomass samples collected from the structured-bed region (Fig. 4a and Table 2) so that a similar trend was associated with the HY (5.23 *vs.* 2.48–3.21 mmol g^{-1}CHt; Table 2). An even higher discrepancy was observed when comparing R_{H2} values, which were over 4.5-fold higher (0.78 *vs.* 0.09–0.17 mmol h^{-1}; Table 2) for the biomass from the FDC. The obtained results clearly indicated that the biomass located in the basal portion of the reactor drives the $bioH_2$ production in the AnSTBR, as a direct result of the prompt availability of sugars. In turn, the sharp decrease in the availability of CHt in the upper portions of the reactor (Section 3.1) most likely favored the establishment of acidogenic populations with lower $bioH_2$-producing capabilities. Differences in the fermentation pH (5.58 *vs.* 4.61–4.66; Table 2) also indicated the most favorable conditions for $bioH_2$ production in systems fed with FDC-derived biomass, based on the optimal pH value (pH = 5.38) previously defined for molasses thermophilic DF [18].

Acidogenic biomass samples collected in different portions of the structured-bed region presented different $bioH_2$ production potential values, associating a 1.5-fold higher P_{H2} to the STB_{UP} compared with the STB_{LP} (Fig. 4a and Table 2). This finding corroborates the patterns observed in the AnSTBR, as metabolite distribution profiles suggested the occurrence of some "residual" hydrogenogenic activity in the upper portion of the structured-bed region (Section 3.1). However, in BPP tests no HBu buildup has been observed (Fig. 4b,c), suggesting the establishment of different $bioH_2$-producing pathways within the batch systems filled with STB_{UP}-derived biomass samples. Comparing reactors filled with STB_{LP}- and STB_{UP}-derived biomass samples (Fig. 4b,c) depicts slightly higher HAc (407 vs. 557 mg-COD L^{-1}; Fig. 4b) and EtOH (685 vs. 866 mg-COD L^{-1}; Fig. 4b) concentrations in the latter, potentially suggesting the contribution of acetic- and ethanol-type fermentation pathway for the increasing $bioH_2$ production levels (Reaction 11). In addition to direct sugar fermentation (Reaction 4), the co-production of HAc, EtOH and $bioH_2$ (Reaction 11) could be pointed out as an alternative pathway to explain the differences observed between STB_{LP} and STB_{UP}, because HBu concentrations reached similar levels (670–627 mg-COD L^{-1}; Fig. 4b) This particular pathway has also been suggested to occur in thermophilic acidogenic systems inoculated with fermented sugarcane vinasse [25], characterizing the metabolite-supported hypothesis as plausible. Conversely, butyrate-type fermentation was most likely the primary $bioH_2$-producing pathway in batch systems inoculated with FDC-derived biomass (Fig. 4b,c), based on HBu concentrations 4–5-fold higher than HAc and EtOH levels. In this case, the observed pattern was slightly different from the one observed in the FDC of the AnSTBR, in which similar production levels were observed for both HBu and HAc (Fig. 2b,c). This discrepancy most likely resulted from differences in the dynamics of fresh substrate (CHt) availability, considering continuous (AnSTBR) and limited (batch reactors) provision patterns. SPMB observed for the batch systems (83.1 ± 1.7%; Fig. 4c) reached equivalent levels to the ones obtained for the continuous system (Fig. 2c).

In practical aspects, the obtained results indicate that approximately a quarter (1.52 h) of the overall HRT (6 h) would be effectively required to attain the $bioH_2$ production levels reported for the AnSTBR [18], using the volume of the FDC (0.48 L; Fig. 1) and the theoretical feeding flow rate (316,67 mL h^{-1}) as calculation references. In other words, BPP tests, in addition to the spatial distribution of metabolites (Fig. 2a,c), suggest that the structured-bed region negligibly contributes to the direct $bioH_2$ production in the AnSTBR, despite the "residual" hydrogenogenic activity identified in the upper portion of the bed. However, the STB might indirectly provide adequate conditions for $bioH_2$ production, by (i) acting as an intermediate barrier to prevent enhanced biomass washout and (ii) favoring the release of the gaseous phase toward the headspace, with both aspects associated with the high porosity intrinsic to STB-based reactors (> 90% [17]). Compared with packed-bed systems, the structured bed retains a lower fraction of the produced biomass (Section 3.2), which prevents excess accumulation of solids within the acidogenic system and the subsequent losses in $bioH_2$ production due to the re-distribution of the metabolic energy for cell maintenance. Moreover, biogas retention within the support material should reach a much lesser extent in the AnSTBR, also in comparison with packed-bed reactors, positively impacting the recovery of the produced

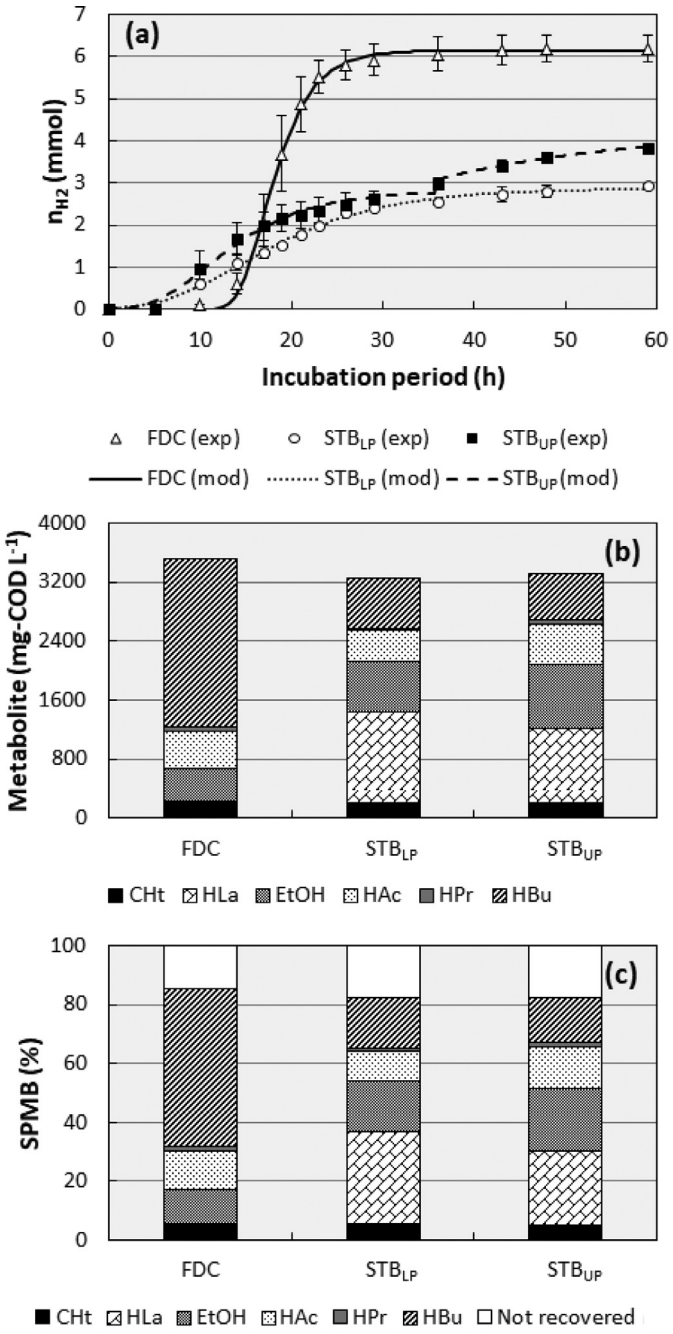

Fig. 4. BPP tests comparing the hydrogenogenic activity of biomass samples from different reactor compartments: (a) molar $bioH_2$ production (exp- experimental values, mod- fitted models), (b) soluble phase metabolites concentration and (c) CODs-based SPMB. Nomenclature: CHt – total carbohydrates, HLa – lactic acid, EtOH – ethanol, HAc – acetic acid, HPr – propionic acid, HBu – butyric acid.

$bioH_2$. Nevertheless, further studies could provide a more accurate scenario regarding the impacts of using smaller STB regions on the overall performance of acidogenic systems.

3.4. Microbial characterization: who drives $bioH_2$ production?

16S rRNA gene amplicon sequencing was used to determine the microbial composition of the biomass at the beginning and by the end of the continuous fermentation in the AnSTBR. The microbial characterization (genus level) of samples collected from the inoculum (naturally fermented sugarcane vinasse; S1), the FDC (suspended biomass S2), the lower (STB_{LP}; S3) and upper (STB_{UP}; S4) portions of the bed region (attached biomass) is depicted in Fig. 5, considering the most representative genera, i.e., relative abundance (RA) ≥ 1%. Samples S2–S4 were obtained at the end of the operating period (320 d). Representative microbial families and genera (RA ≥ 1%) are also summarized in a heat map provided in the Supplementary data section, complementing the microbial analysis. More than 19,000 good-quality reads were obtained for each sample, grouped into ASV and classified using the most recent SILVA 16S rRNA gene reference database (release 138 [43]). Details of sample S1 have been previously presented elsewhere [19], because the same fermentative microbial consortium was used in the inoculation of different DF systems. However, the characterization of S1 will be briefly discussed herein, in an effort to understand the evolution of the microbial differentiation in the AnSTBR.

The characterization at the genus level showed that the community from the inoculum (S1) was different from the other samples. Most of the genera abundant in S1, namely, *Bacillus* (19.6%), *Fonticella* (4.8%), *Clostridium* (7.1%), *Pseudoclostridium* (2.8%), *Tepidimicrobium* (15.4%) and *Lysinibacillus* (10.2%) (Fig. 5) were rarely observed (RA << 1%) in the microbial communities from samples S2–S4. Despite the preliminary growth of groups with optimum growth under thermophilic conditions, which include the $bioH_2$-producing genera *Tepidimicrobium* [44] and *Pseudoclostridium* [45] and the non-$bioH_2$-producing genus *Fonticella* [46], the operating conditions were most likely restrictive to their long-term establishment. The *Clostridium* genus was identified only in the inoculum (Fig. 5), differently from previous reports in which this particular genus participated as a relevant microbial group in (hyper)thermophilic DF systems inoculated with naturally fermented sugarcane vinasse [12,19,25,47,48] in fixed-film reactors.

The distribution of the microbial groups within the different portions of the AnSTBR (Fig. 5) revealed that $bioH_2$ evolution was driven by the *Thermoanaerobacterium* genus, and differences in RA values and in the spatial distribution of the Fe-hydrogenase (*hyd*) gene (Fig. 6) directly explained the discrepant $bioH_2$ production patterns in BPP tests (Section 3.3). The operating conditions applied in the AnSTBR, with emphasis on pH optimization (~5.38) as previously described elsewhere [18], favored the long-term (320 d) establishment of the *Thermoanaerobacterium* genus in the FDC, as observed by the increase in RA values (15.4 *vs.* 1.8%) relative to the inoculum (Fig. 5). $BioH_2$ production from sugars through the acetic- (Reaction 4) and butyric-type (Reaction 5) fermentation pathways prevailed in this case, following the metabolite distribution previously indicated (Section 3.1). The number of copies for the *hyd* gene identified in the FDC was higher than in both portions of the bed region (Fig. 6), corroborating the major participation of the *Thermoanaerobacterium* genus in $bioH_2$ evolution. Interestingly, the highest number of copies for the *hyd* gene was measured in the inoculum (sample S1; Fig. 6), regardless of the low RA associated with the *Thermoanaerobacterium* genus. Despite the sharp long-term microbial differentiation observed in the AnSTBR, this result highlights the $bioH_2$-producing character of the inoculum, considering the participation of the genera *Bacillus, Clostridium, Tepidimicrobium* and *Pseudoclostridium*.

The sharp decrease in CHt availability favored the establishment of non-$bioH_2$-producing populations in the STB_{LP}, also leading to a sharp drop in the RA for the *Thermoanaerobacterium* genus (4.2%; Fig. 5), and thus explaining the lowest BPP observed (Section 3.3; Fig. 4a). In fact, the non-$bioH_2$-producing character of the microbial populations in the STB_{LP} was highlighted by the lowest number of copies for the *hyd* gene identified in sample S3 (Fig. 6). Conversely, lactate production in the STB_{LP} played a key-role to favor the establishment of the *Thermoanaerobacterium* genus in the upper portion of the reactor (RA = 20.3%; Fig. 5), because proper substrate, i.e., HLa in addition to HAc remaining from the FDC, was available to stimulate the hydrogenogenic activity (Reaction 6), as observed by the increase (relative to sample S3) in the number of copies for the *hyd* gene in sample S4 (Fig. 6). These results corroborate previous findings on the thermophilic DF of sugarcane

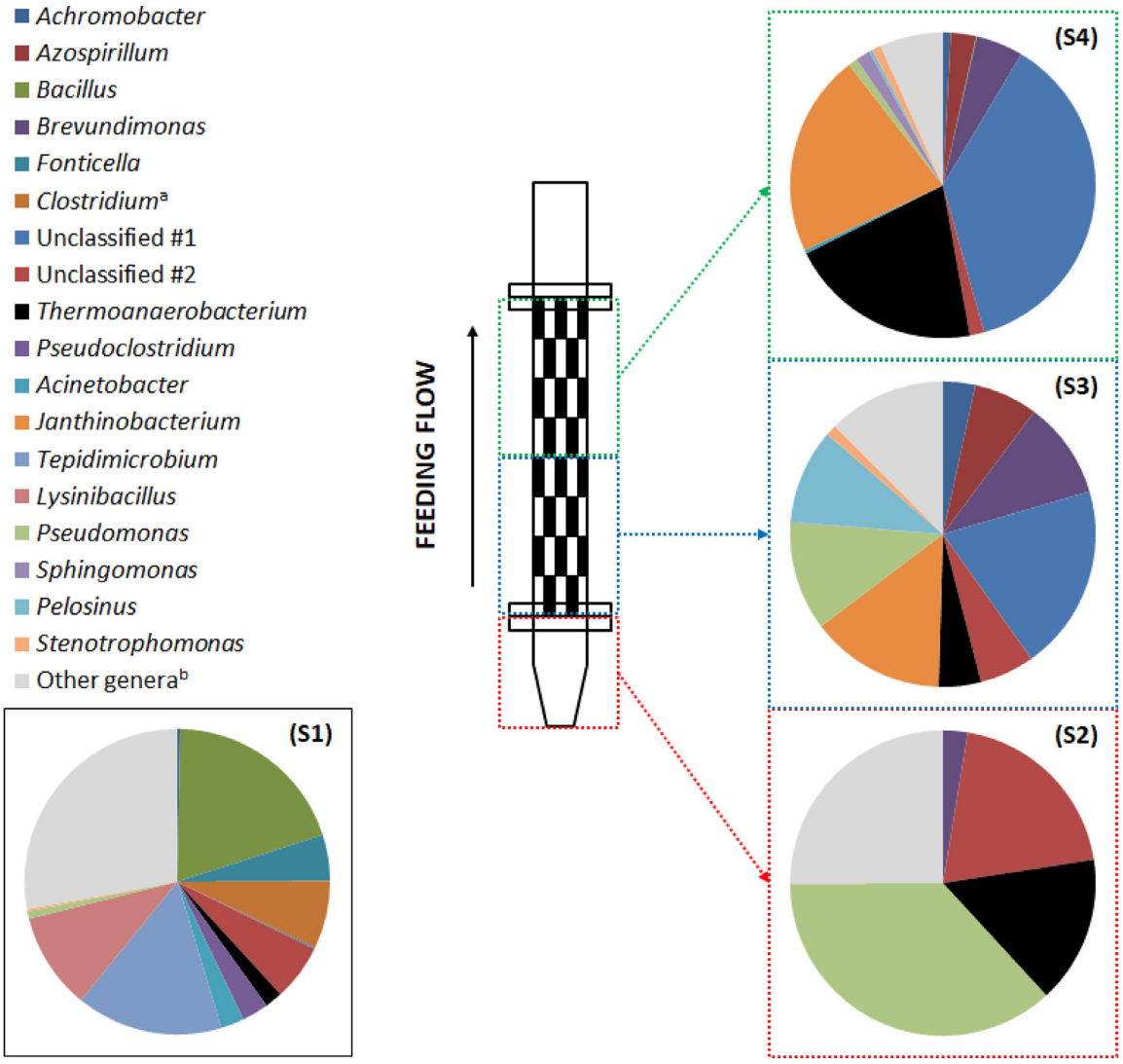

Fig. 5. Microbial characterization at the genus level of the biomass samples collected from the inoculum (S1) and from different portions of the AnSTBR (S2–S4) using 16S rRNA gene amplicon sequencing. Groups with relative abundance (RA) ≥ 1% in at least one sample are shown. Notes: [a]Include the genera *C.* sensu stricto 1 and *C.* sensu stricto 7. [b]Include the genera (maximum RA): *Acidaminococcus* (1.62%; S2), *Bosea* (1.12%; S3), *Caulobacter* (1.04%; S4), *Nocardioides* (2.38%; S4), *Lactobacillus* (0.91%; S1), *Anaerocolumna* (1.86%; S1) and *Sporolactobacillus* (1.46%; S2), in addition to unclassified/uncultured genera. Unclassified genera #1 and #2 belong to the *Comamonadaceae* and *Enterobacteriaceae* families, respectively.

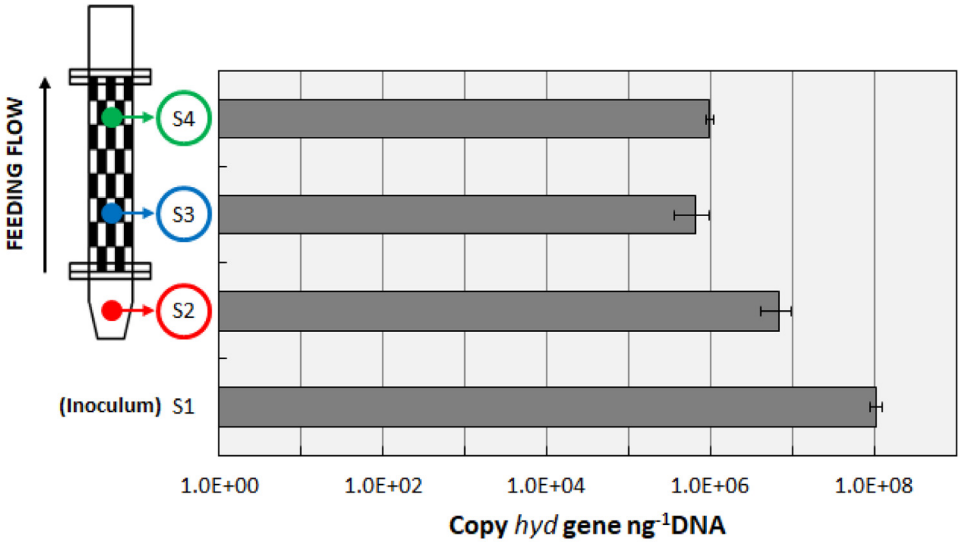

Fig. 6. Copy numbers of Fe-hydrogenase (*hyd*) genes in DNA samples collected from the inoculum (S1) and from different portions of the AnSTBR (S2–S4). The values are the mean of triplicate reactions and error bars represent the standard deviation of the measurements.

molasses [19], in which the participation of the *Thermoanaerobacterium* genus in the uptake of both fresh (sugar-rich) and fermented (HLa- and HAc-rich) substrate was also observed, despite the much higher applied OLR (86 kg-CODt m^{-3} d^{-1}) in that case. This genus has been systematically indicated as the primary $bioH_2$-producing microbial group in the fermentation of sugarcane-derived substrates under high temperatures, e.g., vinasse [12,14,25,47,49], molasses [19,26,50] and bagasse [51,52].

$BioH_2$ evolution could have been complementarily associated with distinct microbial groups in the FDC and in the bed region (STB_{LP} and STB_{UP}). High RA values were associated with the *Pseudomonas* genus in the FDC (36.4%) and STB_{LP} (11.4%), suggesting relevant participation of this group in substrate conversion. Previous studies indicated that *Pseudomonas* sp. may positively impact $bioH_2$ evolution in DF systems, by either supplying $bioH_2$-producing groups with proper substrates or directly producing $bioH_2$ [53-55]. Despite such findings, both the metabolite profile distribution in the AnSTBR (Section 3.1) and the $bioH_2$ evolution patterns in BPP tests (Section 3.3) indicated the potential participation of the *Pseudonomas* genus in parallel conversion pathways, such as HLa production. The relatively simple nutritional and environmental requirements facilitate the overgrowth of the *Pseudomonas* genus relative to other microorganisms [56], which could explain the high RA values, although previous research indicated some growth limitations of *Pseudomonas* sp. within the thermophilic temperature range [25]. In particular, the *Pseudomonas* genus is frequently found in different sugarcane-derived products, such as vinasse [57] and molasses [58], so its introduction and further establishment in the AnSTBR may have occurred naturally through fresh molasses supplying.

A high RA associated with the *Enterobacteriaceae* family (19.7%, unclassified genus #2; Fig. 5) was also observed in the FDC, with decreasing levels in the upper portions of the reactor, i.e., 5.7% (STB_{LP}) and 1.5% (STB_{UP}) (Fig. 5). This group was also identified in the inoculum, i.e., sample S1 (RA = 5.9%; Fig. 5). The *Enterobacteriaceae* family presents favorable characteristics towards efficient $bioH_2$ production, such as the capability to withstand high hydrogen partial pressure levels allied to an enzymatic/metabolic versatility, because most individuals have either [FeFe] hydrogenase or formate hydrogen lyase (FHL) enzymes [59]. Hence, the $bioH_2$-producing potential of *Enterobacter* sp. [60], *Klebsiella* sp. [61] and *Citrobacter* sp. [62] is commonly assessed; however, most studies are carried out under mesophilic temperature conditions (<40 °C). Similar to the *Pseudomonas* genus, previous studies also reported on growth limitations of individuals belonging to the *Enterobacteriaceae* family at high temperature (55–70 °C [25]), which hinders defining the potential metabolic roles of this group in the AnSTBR. Apart from this "environmental inconsistency", the establishment of the *Enterobacteriaceae* family-related group most likely contributed to maintaining an oxygen-free environment in the AnSTBR, directly favoring the activity of obligate anaerobes, such as the *Thermoanaerobacterium* genus. Hung et al. [63] previously attributed this role to *Klebsiella oxytoca* in a $bioH_2$-producing agitated granular sludge bed reactor, because variations in the participation of this group did not significantly impact the hydrogenogenic activity.

The *Janthinobacterium* genus (*Oxalobacteraceae* family), which was identified in both portions of the bed region (samples S3 and S4, RA = 14.1–21.3%; Fig. 5), may have also contributed to $bioH_2$ evolution in the AnSTBR. This group has been previously identified in hydrogenogenic DF systems under both mesophilic [54,64] and thermophilic [65] conditions fed with different types of substrate, i.e., glucose and starch. Despite such findings, the results obtained in BPP tests (Section 3.3) suggest a minor participation of the *Janthinobacterium* genus in $bioH_2$ production, because the lowest HY values, i.e., 2.48 (STB_{LP}) and 3.21 (STB_{UP}) mmol g^{-1}CHt (Table 2) were observed in reactors inoculated with biomass samples collected from the bed region. Apart from $bioH_2$ production, *Janthinobacterium* sp. is notably known to participate in denitrification processes [66], in which the hydrogenotrophic pathway [67] could imply the consumption of $bioH_2$ and explain the lower HY levels.

However, the *Janthinobacterium* genus most likely participated in the capnophilic production of HLa, following previous findings on the CO_2-driven growth of *Janthinobacterium lividum* strain MTR by Valdes et al. [68]. These authors revealed one of the mechanisms related to the capnophilic behavior, i.e., growth on a CO_2-rich environment, of this bacterial strain when colonizing the skin of amphibians. Despite the clear differences between growth conditions in an acidogenic reactor (anaerobic, high acidity) and on a skin (aerobic), Valdes et al. [68] indicated that different mechanisms explain the capnophilic behavior of individuals belonging to the *Janthinobacterium* genus, which supports the hypothesis. This hypothesis is strengthened by the identification neither of the *Thermotoga* genus in the microbial samples, which has been notably characterized to mediated CLF (Reaction 7 [28–30]), nor of any other recognizably HLa-producing genus (Fig. 5). For instance, the *Lactobacillus* genus minimally participated in the composition of the microbial samples (RA < 0.91%), reaching a null RA value in the STB_{UP}. In fact, the simultaneous establishment of efficient $bioH_2$-producing conditions coupled to the buildup of HLa in the liquid phase (Figs. 2a and 4b) is clear evidence of the occurrence of non-conventional (i.e., sugar-independent) lactic activity in the AnSTBR and, therefore, the detection of HLa in a lactate-producing bacteria-free reactor was explained. This is the first mention of the capnophilic behavior of the *Janthinobacterium* genus in a $bioH_2$-producing system.

Individuals belonging to the *Comamonadaceaea* family (unclassified genus #1) and the genera *Brevundimonas, Azospirillum* and *Pelosinus* corresponded to additional representative microbial groups identified in biomass samples collected from the bed region (S3 and S4; Fig. 5). Previous studies indicated the ability of some of these groups to ferment different types of sugars and produce $bioH_2$, such as the *Brevundimonas* and *Pelosinus* genera [69–70]. However, the spatial distribution of metabolites (Fig. 2a) and the $bioH_2$ evolution patterns in BPP tests (Fig. 4b) suggested a minor participation of these genera in the hydrogenogenic activity in the AnSTBR, because of the low availability of CHt in the upper portions of the system. The lower number of copies for the *hyd* gene in the bed region (relative to the FDC) corroborates this hypothesis (Fig. 6). The *Azospirillum* genus recognizably participates in the biological fixation of nitrogen [71], and therefore was not associated with $bioH_2$ evolution. Similarly, members of the *Comamonadaceae* family were most likely not involved in $bioH_2$ production. This family includes mainly individuals with aerobic heterotrophic metabolism, in addition to some denitrifying members capable of using nitrate or Fe(III) as electron acceptors, and thiosulfate-oxidizing groups that grow autotrophically on hydrogen [72]. The thermophilic conditions applied in the AnSTBR could have favored the *Tepidicella* genus, the only thermophile (optimal growth at 45 °C) currently associated with the *Comamonadaceae* family [73]. However, the non-fermentative character of this genus limits defining any metabolic roles of this group in the AnSTBR.

Hence, the microbial characterization of the AnSTBR provided two distinct scenarios: while $bioH_2$ evolution patterns were fully understood (Fig. 7) through correlating the identification of the *Thermoanaerobacterium* genus with the distribution of both metabolite and *hyd*, the metabolic roles of non-$bioH_2$-producing populations still deserves further clarification in acidogenic systems. Except for the *Janthinobacterium* genus, which was strongly associated with CLF (Fig. 7), numerous genera identified in the reactor notably grew under relatively non-favorable conditions (e.g. high temperature coupled to anaerobiosis). Interestingly, several microbial groups associated with nitrogen cycling, such as the *Comamonadaceae* family and the genera *Azospirillum* and *Janthinobacterium*, were identified, potentially indicating that understanding the fate of nitrogen in such systems may clarify the metabolic role of these microbial populations. In fact, previous research using the same source of inoculum revealed a direct dependence of the fermentation pH

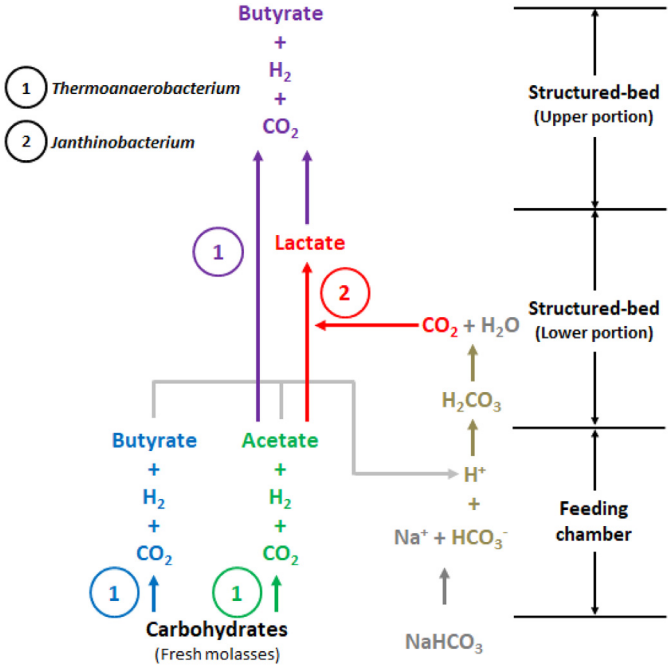

Fig. 7. Primary microbial groups and sequential metabolic pathways associated with the thermophilic fermentation of sugarcane molasses towards the production of bioH_2, butyrate, acetate and lactate.

on the amount of nitrogen available in the substrate [18], which supports the results obtained herein and indicates the way to be followed in further research.

3.5. Next steps: from lab to full-scale applications

In addition to understanding the role of unexpected microbial groups in fermentative systems, future studies on the production of bioH_2 from molasses, as well as from other substrates, should deal with a better characterization of biomass distribution within the reactors, focusing on quantitative aspects. While methods assessing metabolite distribution and the prevailing microbial groups significantly evolved in last years, describing the precise concentration of cells in a specific point of fixed-film reactors is still challenging. Because the levels of substrate availability directly impact the prevailing fermentation pathways [5,6,8,10,16], knowing the amount of retained biomass may be *sine qua non* for defining and applying strategies to improve production levels of bioH_2 (or any other metabolite from substrate fermentation). Proposing the sOLR [5] has greatly contributed to provide a preliminary understanding on such aspects, so the further segmented approach used herein was crucial for attaining more realistic values for the substrate availability along the reactor, considering differences in biomass distribution. However, the calculation of the sOLR still depends on a retroactive approach, i.e., the results are obtained only once the operation of the reactor is stopped. Proposing methods that enable real-time measurements of the sOLR, such as those used in conventional monitoring approaches is, therefore, required. From a practical point of view, this will only be achieved through a precise real-time monitoring of biomass distribution, as previously indicated.

Differently from methanogenic systems, key-aspects (such as the one aforementioned) still require proper consideration before DF systems achieve an attractive technology readiness level, which implies maximizing bioH_2 production within the context of this study. Research efforts conducted in parallel to those presented herein indicated optimal conditions to maximize the thermophilic bioH_2 production from sugarcane molasses [19], as similarly carried out for sugarcane vinasse in previous investigations [14,16]. Yet, some process requirements may fully hamper the economic performance of molasses-fed DF systems, such as dosing $NaHCO_3$ [74]. Managing hydrogen is equally challenging, because of its high flammability and the consequent high costs required in the construction of pipelines and related structures [75]. Alternatively, recovering liquid phase metabolites may also be exploited in acidogenic systems, as recently proposed for vinasse [76]. In this case, efficiently producing target metabolites should be less restrictive than maximizing bioH_2 evolution. Because hydrogen plays the role of an essential electron donor in numerous steps within the anaerobic process [77], minimal disturbance events (e.g. establishing sOLR values out of the optimal range) may severely hinder the hydrogenogenic activity. Hence, a short-to-medium term application of DF may strictly focus on providing a highly fermented substrate for methanogenic systems prior to implementing cost-competitive technologies that ensure efficient production, management and utilization of bioH_2. While boosting methane production by minimizing negative effects of enhanced VFA production in a methanogens-rich environment [74,78], this approach should shorten the way towards the full-scale production of bioH_2 by only requiring modifications in the operating strategies of DF and the update of downstream biogas processing when feasible.

4. Conclusions

Applying a compartmentalized assessment of acidogenesis to a fixed-film system provided a more accurate picture of the dynamics of substrate conversion and cell retention. Analyzing the spatial distribution of metabolites indicated the determining role of acetic-type fermentation to both the bioH_2 evolution and the production of lactate, which was not observed by only assessing the butyrate-rich/acetate-poor effluent stream. In quantitative terms, assessing the specific organic loading rate in individual regions of the system indicated highly favorable conditions of substrate availability (3.71 ± 1.13 g-COD g^{-1}VSS d^{-1}) for bioH_2-producing populations, such as the *Thermoanaerobacterium* genus, in the basal portion, whilst the conventional calculation suggested limiting conditions of substrate (1.41 ± 0.38 g-COD g^{-1}VSS d^{-1}). Overall, comparing the results with previous reports suggests that OLR levels strongly determine the regions of enhanced lactate production within the reactor, which will further direct the relevance of secondary lactate-producing/consuming pathways and the associated microbial groups. The *Janthinobacterium* genus most likely mediated the capnophilic lactic fermentation in the bed region of the reactor, whilst the *Lactobacillus* genus negligibly participated in the lactic activity. Conversely, bioH_2-producing populations in the basal portion majorly contributed to the hydrogenogenic activity (via acetate- and butyrate-type fermentations), irrespective of the OLR level.

Declaration of Competing Interests

The authors declare that they have no known competing financial interests or personal relationships that could have appeared to influence the work reported in this paper.

Acknowledgments

This work was supported by the São Paulo Research Foundation (FAPESP) [grant numbers 2017/00080–5, 2015/50684-9, 2015/06246-7 and 2014/50279-4]; and the Coordination for the Improvement of Higher Education Personnel via the Academic Excellence Program (PROEX-CAPES).

Supplementary materials

Supplementary material associated with this article can be found, in the online version, at doi:10.1016/j.ceja.2021.100125.

References

[1] E. Elbeshbishy, B.R. Dhar, G. Nakhla, H.S. Lee, A critical review on inhibition of dark biohydrogen fermentation, Renew. Sustain. Energy Rev. 79 (2017) 656–668, doi:10.1016/j.rser.2017.05.075.

[2] A. Ghimire, L. Frunzo, F. Pirozzi, E. Trably, R. Escudie, P.N.L. Lens, et al., A review on dark fermentative biohydrogen production from organic biomass: process parameters and use of by-products, Appl. Energy 144 (2015) 73–95, doi:10.1016/j.apenergy.2015.01.045.

[3] G. Kumar, A. Mudhoo, P. Sivagurunathan, D. Nagarajan, A. Ghimire, C.H. Lay, et al., Recent insights into the cell immobilization technology applied for dark fermentative hydrogen production, Bioresour. Technol. 219 (2016) 725–737 http://dx.doi.org/, doi:10.1016/j.biortech.2016.08.065.

[4] S.D. Gomes, L.T. Fuess, E.D. Penteado, S.D.M. Lucas, J.T. Gotardo, M. Zaiat, The application of an innovative continuous multiple tube reactor as a strategy to control the specific organic loading rate for biohydrogen production by dark fermentation, Bioresour. Technol. 197 (2015) 201–207, doi:10.1016/j.biortech.2015.08.077.

[5] M.P. Anzola-Rojas, S.G. Fonseca, C.C. Silva, V.M. Oliveira, M. Zaiat, The use of the carbon/nitrogen ratio and specific organic loading rate as tools for improving biohydrogen production in fixed-bed reactors, Biotechnol. Rep. 5 (2015) 46–54, doi:10.1016/j.btre.2014.10.010.

[6] V.M.C. Blanco, L.T. Fuess, M. Zaiat, Calcium dosing for the simultaneous control of biomass retention and the enhancement of fermentative biohydrogen production in an innovative fixed-film bioreactor, Int. J. Hydrogen Energy 42 (2017) 12181–12196, doi:10.1016/j.ijhydene.2017.02.180.

[7] C. Dinamarca, R. Bakke, Apparent hydrogen consumption in acid reactors: observations and implications, Water Sci. Technol. 59 (7) (2009) 1441–1447, doi:10.2166/wst.2009.135.

[8] L.T. Fuess, L.S.M. Kiyuna, M.L. Garcia, M. Zaiat, Operational strategies for long-term biohydrogen production from sugarcane stillage in continuous acidogenic packed-bed reactor, Int. J. Hydrogen Energy 41 (2016) 8132–8145, doi:10.1016/j.ijhydene.2015.10.143.

[9] G. Peixoto, N.K. Saavedra, M.B. Varesche, M. Zaiat, Hydrogen production from soft-drink wastewater in an upflow anaerobic packed-bed reactor, Int. J. Hydrogen Energy 36 (15) (2011) 8953–8966, doi:10.1016/j.ijhydene.2011.05.014.

[10] H. Hafez, G. Nakhla, M.H. El. Naggar, E. Elbeshbishy, B Baghchehsaraee, Effect of organic loading on a novel hydrogen bioreactor, Int. J. Hydrogen Energy 35 (1) (2010) 81–92, doi:10.1016/j.ijhydene.2009.10.051.

[11] N.M.C. Saady, Homoacetogenesis during hydrogen production by mixed cultures dark fermentation, Int. J. Hydrogen Energy 38 (2013) 13172–13191, doi:10.1016/j.ijhydene.2013.07.122.

[12] A.D.N. Ferraz Junior, C. Etchebehere, M Zaiat, High organic loading rate on thermophilic hydrogen production and metagenomic study at an anaerobic packed-bed reactor treating a residual liquid stream of a Brazilian biorefinery, Bioresour. Technol. 186 (2015) 81–88, doi:10.1016/j.biortech.2015.03.035.

[13] D.M. Fontes Lima, W.K. Moreira, M Zaiat, Comparison of the use of sucrose and glucose as substrate for hydrogen production in an upflow anaerobic fixed-bed reactor, Int. J. Hydrogen Energy 38 (35) (2013) 15074–15083, doi:10.1016/j.ijhydene.2013.09.003.

[14] A.D.N. Ferraz Junior, J. Wenzel, C. Etchebehere, M Zaiat, Effect of organic loading rate on hydrogen production from sugarcane vinasse in thermophilic acidogenic packed bed reactors, Int. J. Hydrogen Energy 39 (3) (2014) 16852–16862, doi:10.1016/j.ijhydene.2014.08.017.

[15] V. Perna, J. Castelló E Wenzel, C. Zampol, D.M. Fontes Lima, L. Borzacconi, et al., Hydrogen production in an upflow anaerobic packed bed reactor used to treat cheese whey, Int. J. Hydrogen Energy 38 (1) (2013) 54–62, doi:10.1016/j.ijhydene.2012.10.022.

[16] L.T. Fuess, M. Zaiat, C.A.O. Nascimento, Novel insights on the versatility of biohydrogen production from sugarcane vinasse via thermophilic dark fermentation: impacts of pH-driven operating strategies on acidogenesis metabolite profiles, Bioresour. Technol. 286 (2019) 121379, doi:10.1016/j.biortech.2019.121379.

[17] S. Aquino, L.T. Fuess, E.C. Pires, Media arrangement impacts cell growth in anaerobic fixed-bed reactors treating sugarcane vinasse: structured vs. randomic biomass immobilization, Bioresour. Technol. 235 (2017) 219–228, doi:10.1016/j.biortech.2017.03.120.

[18] L.T. Fuess, M. Zaiat, C.A.O. Nascimento, Molasses vs. juice: maximizing biohydrogen production in sugarcane biorefineries to diversify renewable energy generation, J. Water Process. Eng. 37 (2020) 101534, doi:10.1016/j.jwpe.2020.101534.

[19] L.T. Fuess, L. Fuentes, P. Bovio-Winkler, F. Eng, C. Etchebehere, M. Zaiat, et al., Full details on continuous biohydrogen production from sugarcane molasses are unraveled: performance optimization, self-regulation, metabolic correlations and quanti-qualitative biomass characterization, Chem. Eng. J. 414 (2021) 128934, doi:10.1016/j.cej.2021.128934.

[20] M.H. Zwietering, I. Jongenburger, F.M. Rombouts, K. van't Riet, Modeling of the bacterial growth curve, Appl. Environ. Microbiol. 56 (6) (1990) 1875–1881.

[21] APHA, AWWA, WEFStandard Methods for the Examination of Water and Wastewater, 22nd ed., APHA, Washington, DC, 2012.

[22] M. Dubois, K.A. Gilles, J.K. Hamilton, P.A. Rebers, F. Smith, Colorimetric methods for determination of sugar and related substance, Anal. Chem. 28 (3) (1956) 350–356, doi:10.1021/ac60111a017.

[23] K.A.C.C. Taylor, A simple colorimetric assay for muramic acid and lactic acid, Appl. Biochem. Biotechnol. 56 (1) (1996) 49–58, doi:10.1007/BF02787869.

[24] M.A.T. Adorno, J.S. Hirasawa, M.B.A. Varesche, Development and validation of two methods to quantify volatile acids (C2-C6) by GC/FID: headspace (automatic and manual) and liquid-liquid extraction (LLE), Am. J. Anal. Chem. 5 (2014) 406–414 http://dx.doi.org/, doi:10.4236/ajac.2014.57049.

[25] L.T. Fuess, A.D.N. Ferraz Junior, C.B. Machado, M Zaiat, Temporal dynamics and metabolic correlation between lactate-producing and hydrogen-producing bacteria in sugarcane vinasse dark fermentation: the key role of lactate, Bioresour. Technol. 247 (2018) 426–433, doi:10.1016/j.biortech.2017.09.121.

[26] C.A. Oliveira, L.T. Fuess, L.A. Soares, M.H.R.Z. Damianovic, Thermophilic biohydrogen production from sugarcane molasses under low pH: metabolic and microbial aspects, Int. J. Hydrogen Energy 45 (7) (2020) 4182–4192, doi:10.1016/j.ijhydene.2019.12.013.

[27] M. Matsumoto, Y. Nishimura, Hydrogen production by fermentation using acetic acid and lactic acid, J. Biosci. Bioeng. 103 (2007) 236–241, doi:10.1263/jbb.103.236.

[28] L. Dipasquale, G. d'Ippolito, A. Fontana, Capnophilic lactic fermentation and hydrogen synthesis by *Thermotoga neopolitana*: an unexpected deviation from the dark fermentation model, Int. J. Hydrogen Energy 39 (10) (2014) 4857–4862, doi:10.1016/j.ijhydene.2013.12.183.

[29] N. Pradhan, L. Dipasquale, G. d'Ippolito, A. Fontana, A. Panico, F. Pirozzi, et al., Model development and experimental validation of capnophilic lactic fermentation and hydrogen synthesis by *Thermotoga neapolitana*, Water Res. 99 (2016) 225–234, doi:10.1016/j.watres.2016.04.063.

[30] N. Pradhan, G. d'Ippolito, L. Dipasquale, G. Esposito, A. Panico, P.N.L. Lens, et al., Simultaneous synthesis of lactic acid and hydrogen from sugars via capnophilic lactic fermentation by *Thermotoga neapolitana cf capnolactica*, Biomass Bioenergy 125 (2019) 17–22, doi:10.1016/j.biombioe.2019.04.007.

[31] T. Iino, A. Manome, S. Okada, T. Uchimura, K. Komagata, Effects of sodium acetate on the production of stereoisomers of lactic acid by *Lactobacillus sakei* and other lactic acid bacteria, J. Gen. Appl. Microbiol. 47 (5) (2001) 223–239, doi:10.2323/jgam.47.223.

[32] T. Iino, T. Uchimura, K. Komagata, The effect of sodium acetate on the growth yield, the production of L- and D-lactic acid, and the activity of some enzymes of the glycolytic pathway of *Lactobacillus sakei* NRIC 1071^T and *Lactobacillus plantarum* NRIC 1067^T, J. Gen. Appl. Microbiol. 48 (2) (2002) 91–102, doi:10.2323/jgam.48.91.

[33] T. Iino, T. Uchimura, K. Komagata, The effect of sodium acetate on the activity of L- and D-lactate hydrogenases in *Lactobacillus sakei* NRIC 1071^T and other lactic acid bacteria, J. Gen. Appl. Microbiol. 49 (1) (2003) 51–58, doi:10.2323/jgam.49.51.

[34] W.C. Khor, H. Roume, M. Coma, H. Vervaeren, K. Rabaey, Acetate accumulation enhances mixed culture fermentation of biomass to lactic acid, Appl. Microbiol. Biotechnol. 100 (2016) 8337–8348, doi:10.1007/s00253-016-7578-5.

[35] R.P. Johnston Jr, E.M. Kesler, R.D McCarthy, Absorption of organic acids from the omasum, J. Dairy Sci. 44 (2) (1961) 331–339, doi:10.3168/jds.S0022-0302(61)89738-5.

[36] M. Kleiber, A.T. Black, M.A. Brown, J. Luick, C.F. Baxter, B.M. Tolbert, Butyrate as a precursor of milk constituents in the intact dairy cow, J. Biol. Chem. 210 (1) (1954) 239–247.

[37] W. Fu, A.P. Mathews, Lactic acid production from lactose by *Lactobacillus plantarum*: kinetic model and effects of pH, substrate, and oxygen, Biochem. Eng. J. 3 (3) (1999) 163–170, doi:10.1016/S1369-703X(99)00014-5.

[38] M.T. Madigan, J.M. Martinko, K.S. Bender, D.H. Buckley, D.A. Stahl, Brock Biology of Microorganisms, 14th ed., Pearson College Division, Boston, 2014.

[39] M.P. Anzola-Rojas, M. Zaiat, H. De Wever, Improvement of hydrogen production via ethanol-type fermentation in an anaerobic down-flow structured bed reactor, Bioresour. Technol. 202 (2016) 42–49, doi:10.1016/j.biortech.2015.11.084.

[40] J.L. Tholozan, J.P. Touzel, E. Samain, J.P. Grivet, G. Prensier, G. Albagnac, *Clostridium neopropionicum* sp. nov., a strict anaerobic bacterium fermenting ethanol to propionate through acrylate pathway, Arch. Microbiol. 157 (3) (1992) 249–257, doi:10.1007/BF00245158.

[41] M.P. Anzola-Rojas, M. Zaiat, A novel anaerobic down-flow structured-bed reactor for long-term stable H2 energy production from wastewater, J. Chem. Technol. Biotechnol. 91 (5) (2016) 1551–1561, doi:10.1002/jctb.4754.

[42] Y.J. Chan, M.F. Chong, C.L. Law, D.G. Hassell, A review on anaerobic-aerobic treatment of industrial and municipal wastewater, Chem. Eng. J. 155 (1–2) (2009) 1–18, doi:10.1016/j.cej.2009.06.041.

[43] C. Quast, E. Pruesse, P. Yilmaz, J. Gerken, T. Schweer, P. Yarza, et al., The SILVA ribosomal RNA gene database project: improved data processing and web-based tools, Nucleic. Acids. Res. 41 (D1) (2013) D590–D596, doi:10.1093/nar/gks1219.

[44] A. Slobodkin, Tepidimicrobium, in: ME Trujillo, S Dedysh, P DeVos, B Hedlund, P Kämpfer, FA Rainey (Eds.), Bergey's Manual of Systematics of Archaea and Bacteria, 2017, doi:10.1002/9781118960608.gbm01399.

[45] X. Zhang, B. Tu, L. Dai, P.A. Lawson, Z. Zheng, L.Y. Liu, et al., *Petroclostridium xylanilyticum* gen. nov., sp. nov., a xylan-degrading bacterium isolated from an oilfield, and reclassification of clostridial cluster III members into four novel genera in a new *Hungateiclostridiaceae* fam. nov, Int. J. Syst. Evol. Microbiol. 68 (10) (2018) 3197–3211, doi:10.1099/ijsem.0.002966.

[46] B. Fraj, W.B. Hania, A. Postec, M. Hamdi, B. Ollivier, M.L. Fardeau, *Fonticella tunisiensis* gen. nov., sp. nov., isolated from a hot spring, Int. J. Syst. Evol. Microbiol. 63 (6) (2013) 1947–1950, doi:10.1099/ijs.0.041947-0.

[47] M.Y.K. Niz, I. Etchelet, L. Fuentes, C. Etchebehere, M. Zaiat, Extreme thermophilic condition: an alternative for long-term biohydrogen production from sugarcane vinasse, Int. J. Hydrogen Energy 44 (41) (2019) 22876–22887, doi:10.1016/j.ijhydene.2019.07.015.

[48] R. Vilela, F.T. Saia, G.B. Gregoracci, R. Duarte, P. Andrade, B. van der Zaan, et al., Hydrogen production in reactors: the influence of organic loading rate, inoculum and support material, Int. J. Hydrogen Energy 44 (50) (2019) 27259–27271, doi:10.1016/j.ijhydene.2019.08.180.

[49] S.C. Santos, P.R.F. Rosa, I.K. Sakamoto, M.B.A. Varesche, E.L. Silva, Continuous thermophilic hydrogen production and microbial community analysis from anaerobic

digestion of diluted sugar cane stillage, Int. J. Hydrogen Energy 39 (17) (2014) 9000–9011, doi:10.1016/j.ijhydene.2014.03.241.
[50] P. Kongjan, S. O-Thong, I. Angelidaki, Hydrogen and methane production from desugared molasses using a two-stage thermophilic anaerobic process, Eng. Life Sci. 13 (2) (2013) 118–125, doi:10.1002/elsc.201100191.
[51] J. Cheng, M. Zhu, A novel anaerobic co-culture system for bio-hydrogen production from sugarcane bagasse, Bioresour. Technol. 144 (2013) 623–631 http://dx.doi.org/, doi:10.1016/j.biortech.2013.07.018.
[52] L.A. Soares, J.K. Braga, F. Motteran, I.K. Sakamoto, P.A.S. Monteiro, P. Seleghim Jr, et al., Bioconversion of sugarcane bagasse into value-added products by bioaugmentation of endogenous cellulolytic and fermentative communities, Waste Biomass Valor 10 (2019) 1899–1912, doi:10.1007/s12649-018-0201-5.
[53] J. Yun, K.S. Cho, Effects of organic loading rate on hydrogen and volatile fatty acid production and microbial community during acidogenic hydrogenesis in a continuous stirred tank reactor using molasses wastewater, J. Appl. Microbiol. 121 (6) (2015) 1627–1636, doi:10.1111/jam.13316.
[54] Z.D. Alvarado-Cuevas, A.M. López-Hidalgo, L.G. Ordoñez, E. Oceguerra-Contreras, J.T. Ornelas-Salas, A. De León-Rodríguez, Biohydrogen production using psychrophilic bacteria isolated from Antarctica, Int. J. Hydrogen Energy 40 (24) (2015) 7586–7592, doi:10.1016/j.ijhydene.2014.10.063.
[55] N. Fakhimi, A. Dubini, O. Tavakoli, D. González-Ballester, Acetic acid is key for synergetic hydrogen production in Chlamydomonas-bacteria co-cultures, Bioresour. Technol. 289 (2019) 121648, doi:10.1016/j.biortech.2019.121648.
[56] K.N. Timmis, *Pseudomonas putida*: a cosmopolitan opportunist *par excellence*, Environ. Microbiol. 4 (12) (2002) 779–781, doi:10.1046/j.1462-2920.2002.00365.x.
[57] N.A. Cassman, K.S. Lourenço, J.B. Carmo, H. Cantarella, E.E. Kuramae, Genome-resolved metagenomics of sugarcane vinasse bacteria, Biotechnol. Biofuels 11 (2018) 48, doi:10.1186/s13068-018-1036-9.
[58] N. Naheed, N. Jamil, Optimization of biodegradable plastic production on sugar cane molasses in *Enterobacter* sp. SEL2, Braz. J. Microbiol. 45 (2) (2014) 417–426, doi:10.1590/S1517-83822014000200008.
[59] B. Gopalakrishnan, N. Khanna, D Das, Dark-Fermentative Biohydrogen Production, in: A Pandey, SV Mohan, JS Chang, PC Hallenbeck, C Larroche (Eds.), Biomass, Biofuels, Biochemicals: Biohydrogen, 2nd ed., Elsevier, 2019, pp. 79–122, doi:10.1016/B978-0-444-64203-5.00004-6.
[60] R. Rao, N. Basak, Optimization and modelling of dark fermentative hydrogen production from cheese whey by *Enterobacter aerogenes* 2822, Int. J. Hydrogen Energy 46 (2) (2021) 1777–1800, doi:10.1016/j.ijhydene.2020.10.142.
[61] T. Chookaew, S. O-Thong, P. Prasertsan, Fermentative production of hydrogen and soluble metabolites from crude glycerol of biodiesel plant by the newly isolated thermotolerant *Klebsiella pneumoniae* TR17, Int. J. Hydrogen Energy 37 (18) (2012) 13314–13322 http://dx.doi.org/, doi:10.1016/j.ijhydene.2012.06.022.
[62] C. Hamilton, S. Hiligsmann, L. Beckers, J. Masset, A. Wilmotte, P. Thonart, Optimization of culture conditions for biological hydrogen production by *Citrobacter freundii* CWBI952 in batch, sequenced-batch and semicontinuous operating mode, Int. J. Hydrogen Energy 35 (3) (2010) 1089–1098, doi:10.1016/j.ijhydene.2009.10.073.
[63] C.H. Hung, K.S. Lee, L.H. Cheng, Y.H. Huang, P.J. Lin, J.S. Chang, Quantitative analysis of a high-rate hydrogen-producing microbial community in anaerobic agitated granular sludge bed bioreactors using glucose as substrate, Appl. Microbiol. Biotechnol. 75 (2007) 693–701, doi:10.1007/s00253-007-0854-7.
[64] Y.Y. Ning, D.W. Jin, G.P. Sheng, H. Harada, X.Y. Shi, Evaluation of the stability of hydrogen production and microbial diversity by anaerobic sludge with chloroform treatment, Renew. Energy 38 (1) (2012) 253–257, doi:10.1016/j.renene.2011.07.038.
[65] Y. Akutsu, Y.Y. Li, M. Tandukar, K. Kubota, H. Harada, Effects of seed sludge on fermentative characteristics and microbial community structures in thermophilic hydrogen fermentation of starch, Int. J. Hydrogen Energy 33 (22) (2008) 6541–6548, doi:10.1016/j.ijhydene.2008.08.038.
[66] M. Yang, D. Lu, B. Qin, Q. Liu, Y. Zhao, H. Liu, et al., Highly efficient nitrogen removal of a coldness-resistant and low nutrient needed bacterium, *Janthinobacterium* sp. M-11, Bioresour. Technol. 256 (2018) 366–373, doi:10.1016/j.biortech.2018.02.049.
[67] K.A. Karanasios, I.A. Vasiliadou, S. Pavlou, D.V. Vayenas, Hydrogenotrophic denitrification of potable water: a review, J. Hazard. Mater. 180 (1–3) (2010) 20–37, doi:10.1016/j.jhazmat.2010.04.090.
[68] N. Valdes, P. Soto, L. Cottet, P. Alarcon, A. Gonzalez, A. Castillo, et al., Draft genome sequence of *Janthinobacterium lividum* strain MTR reveals its mechanism of capnophilic behavior, Stand. Genomic Sci. 10 (2015) 110, doi:10.1186/s40793-015-0104-z.
[69] A.W. Danial, Abdel-Wahab AM, Arafat HH, Abdel-Basset R. Identification and enhanced hydrogen evolution in two alginate-immobilized strains of *Brevundimonas diminuta* isolated from sludge and waterlogged soil, Ecohydrol. Hydrobiol. 15 (2) (2015) 81–88 http://dx.doi.org/, doi:10.1016/j.ecohyd.2015.04.004.
[70] W.M. Moe, R.E. Stebbing, J.U. Rao, K.S. Bowman, M.F. Nobre, M.S. Costa, et al., *Pelosinus defluvii* sp. nov., isolated from chlorinated solvent-contaminated groundwater, emended description of the genus *Pelosinus* and transfer of *Sporotalea propionica* to *Pelosinus propionicus* comb. nov, Int. J. Syst. Evol. Microbiol. 62 (6) (2012) 1369–1376, doi:10.1099/ijs.0.033753-0.
[71] E.L. Reinhardt, P.L. Ramos, G.P. Manfio, H.R. Barbosa, C. Pavan, C.A. Moreira-Filho, Molecular characterization of nitrogen-fixing bacteria isolated from Brazilian agricultural plants at São Paulo State, Braz. J. Microbiol. 39 (3) (2008) 414–422, doi:10.1590/S1517-83822008000300002.
[72] A. Willems, E. Rosenberg, E.F. DeLong, S. Lory, E. Stackebrandt, F. Thompson, The Family *Comamonadaceae*, in: The Prokaryotes, Springer, Berlin, 2014, pp. 777–851, doi:10.1007/978-3-642-30197-1_238.
[73] L. França, F.A. Rainey, M.F. Nobre, M.S. Costa, *Tepidicella xavieri* gen. nov., sp. nov., a betaproteobacterium isolated from a hot spring runoff, Int. J. Syst. Evol. Microbiol. 56 (4) (2006) 907–912, doi:10.1099/ijs.0.64193-0.
[74] L.T. Fuess, M.M. Araújo Jr, M.L. Garcia, M Zaiat, Designing full-scale biodigestion plants for the treatment of vinasse in sugarcane biorefineries: how phase separation and alkalinization impact biogas and electricity production costs? Chem. Eng. Res. Des. 119 (2017) 209–220, doi:10.1016/j.cherd.2017.01.023.
[75] Nelissen D., Faber J., van der Veen R., van Grinsven A., Shanthi H., van den Toorn E. Availability and costs of liquefied bio- and synthetic methane: The maritime shipping perspective. Report 20.190236.031. Delft, NL: CE Delft; 2020. https://cedelft.eu/publications/availability-and-costs-of-liquefied-bio-and-synthetic-methane/. (Accessed 14 May 2021).
[76] F.E. Sánchez, L.T. Fuess, G.S. Cavalcante, M.A.T. Adorno, M. Zaiat, Value-added soluble metabolite production from sugarcane vinasse within the carboxylate platform: an application of the anaerobic biorefinery beyond biogas production, Fuel 286 (2021) 119378, doi:10.1016/j.fuel.2020.119378.
[77] X. Zhu, P. Zhou, Y. Chen, X. Liu, D. Li, The role of endogenous and exogenous hydrogen in the microbiology of biogas production systems, World. J. Microbiol. Biotechnol. 36 (2020) 79, doi:10.1007/s11274-020-02856-9.
[78] P.A. Cremonez, J.G. Teleken, T.R.W. Meier, H.J. Alves, Two-stage anaerobic digestion in agroindustrial waste treatment: a review, J. Environ. Manage. 281 (2021) 111854, doi:10.1016/j.jenvman.2020.111854.